Energy-Based State-Space Representation of Modular Multilevel Converters with a Constant Equilibrium Point in Steady-State Operation

Gilbert Bergna-Diaz, Jon Are Suul, *Member IEEE*, and Salvatore D'Arco

Abstract— The internal currents and voltages of Modular Multilevel Converters (MMCs) contain multiple frequency components in steady state operation and remain time-periodic even when transformed into a synchronously rotating reference frame. This prevents a straightforward state-space representation where a constant equilibrium point is reached and all state variables converge to constant values under steady-state conditions. Such steady-state time-invariant (SSTI) representations are needed for linearization and eigenvalue-based analysis of small-signal stability. This paper presents an energy-based model of an MMC with a modulation strategy where the insertion indices are compensated for the oscillations in the sum arm voltage. The formulation of the model allows for deriving, by the application of Park transformations at three different frequencies, a SSTI representation that accurately captures the internal dynamics of the MMC. This model can be simplified to a reduced order model that maintains accurate reproduction of the external behavior at the ac- and dc-sides while neglecting some of the internal dynamics. The validity and accuracy of these two SSTI MMC models are verified by time-domain simulations and their utilization for eigenvalue-based analysis of MMC dynamics is demonstrated by examples.

Index Terms— HVDC Transmission, Modular Multilevel Converter, Park Transformations, State-space Modelling

NOMENCLATURE

1) MMC and system variables

i_u, i_l	Current in upper (u) and lower (l) arm
i_c, i_v	Circulating current, and ac grid-side current
w_u, w_l	Aggregated capacitor energy in upper (u) and lower (l) arm
w_Σ, w_Δ	Capacitor energy sum and difference between upper and lower arms

n_u, n_l	Upper and lower arm insertion indexes
v_u^{SMi}, v_l^{SMi}	Voltage of the ith sub-module capacitor in the upper or lower arm
v_u^σ, v_l^σ	Upper and lower arm capacitor voltage sum
v_u, v_l	Upper and lower arm output voltages
u_c, e_v	Voltages driving circulating and ac-side currents
v_o, v_g	Voltage at the point of common coupling and voltage of ac-grid Thévenin equivalent
v_{dc}	Voltage at the dc terminals of the MMC
*	Indicates reference values in the control system

2) Main system parameters

R_a, L_a	MMC arm resistance and inductance
R_f, L_f	Equivalent MMC output resistance and inductance, representing transformer series impedance and any additional filters
C_o	Equivalent capacitance at connection to ac grid
R_{eq}, L_{eq}	Equivalent ac resistance and inductance defined as $R_{eq} = R_a/2 + R_f$, $L_{eq} = L_a/2 + L_f$
R_g, L_g	Equivalent grid-side resistance and inductance
C_{SM}	Capacitance of a MMC sub-module
N	Number of sub-modules in an arm
C_{eq}	Equivalent MMC arm capacitance defined as $C_{eq} = C_{SM}/N$
C_{dc}	Equivalent capacitance at the dc terminals

3) Reference frame orientations

abc	Natural three-phase coordinates
$dqz_{-2\omega}$	Synchronous reference frame rotating at -2ω
$dqz_{+\omega}$	Synchronous reference frame rotating at $+\omega$
$dq_{+3\omega}$	Synchronous reference frame rotating at $+3\omega$

I. INTRODUCTION

The Modular Multilevel Converter (MMC) is emerging as a preferred topology for Voltage Source Converter (VSC) -based HVDC transmission schemes [1]-[5]. However, the modelling and the control of the MMC is in general more challenging than for two- or three-level VSC configurations, since the MMC is characterized by a high number of independent switching elements and by additional internal dynamics related to the circulating currents flowing through the submodules of each phase [6]. Moreover, each phase of an MMC behaves as a single-phase multi-level converter, where the double frequency oscillations in the power flow cause corresponding fluctuations in the sub-module capacitor voltages. Thus, even in steady state operation, the internal currents and voltages of an MMC will contain multiple frequency components [7].

Significant efforts have recently been dedicated towards modelling and analysis of the MMC topology and its control.
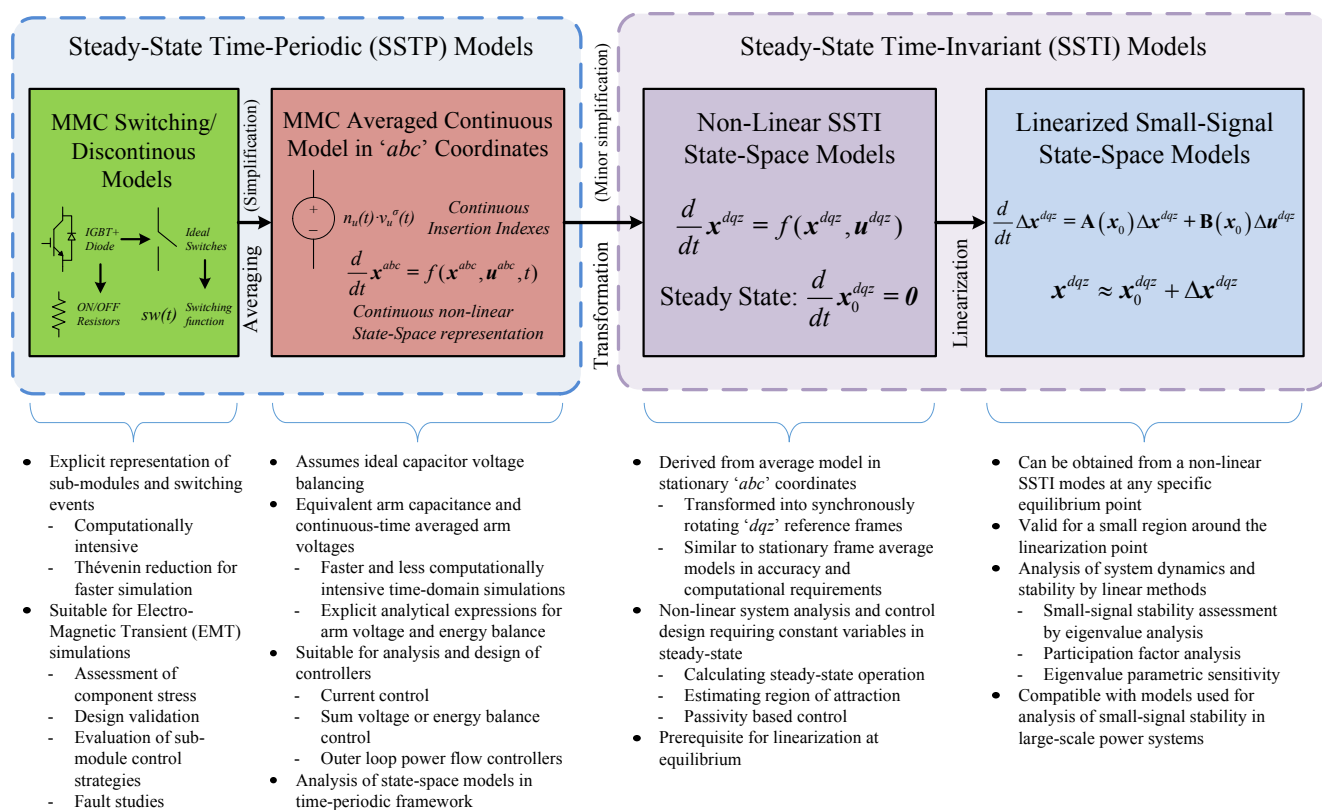
Fig. 1 Overview of MMC modelling approaches and their areas of application

An overview of different types of models, how they originate from the MMC topology and their typical range of application is shown in Fig. 1. Indeed, detailed switching models with explicit representation of all sub-module capacitors of an MMC, including models with Thévenin equivalent representation of each arm according to [8], are intended for time-domain simulations. If the individual representation of each sub-module capacitor voltage is not necessary, simplified switching function models can be introduced to reduce the required simulation time [9], [10].

Continuous time average models can be obtained by approximating the switching effects with a continuous signal and assuming perfect balancing between the sub-module capacitor voltages [6], [7], [11] ,[12]. Such average models allow for efficient time-domain simulation and lead to simple analytical expressions for representing each arm of an MMC. Thus, they are commonly utilized in mathematical analysis for control system design and for understanding the internal dynamics of each phase of the MMC. Since such models represent the phase and arm quantities of the MMC, steady-state operation is characterized by an orbit of the state-space variables and not by a constant equilibrium point. Thus, the models will inherently have Steady-State Time-Periodic (SSTP) characteristics, as indicated in the left part of Fig. 1. Stability analysis based on SSTP average models requires advanced methods specifically developed for time-periodic systems, as recently applied to an MMC in [13].

Although the various SSTP models indicated to the left of Fig. 1 are suitable for most purposes related to time-domain simulation and controller design, or for dynamic analysis of

each arm or phase of an MMC, they are not easily applicable in established methods for system-oriented analysis. Indeed, SSTP average models of MMCs cannot be linearized and utilized for traditional eigenvalue-based analysis commonly applied in studies of small-signal stability of power systems [14]. Instead, methods for system analysis that depend on linearization, as well as many established techniques for non-linear stability assessment or control system design, assume as a prerequisite the availability of a state-space model where all stable operating points are characterized by an equilibrium point and all state variables converge to constant values in steady state operation [14], [15]. Thus, models to be utilized for such purposes should have Steady-State Time-Invariant (SSTI) characteristics.

While SSTI representations of two-level VSCs can be easily derived by applying the Park transformation, the multiple frequency components appearing in the arm currents and capacitor voltages of the MMC prevent SSTI representation by transformation into a single Synchronous Reference Frame (SRF). Thus, derivation of MMC models with SSTI characteristics is still object of research. Fig. 1 indicates how such SSTI-models should be derived from a corresponding SSTP average model by applying appropriate reference frame transformation and simplifications. The figure also shows how a non-linear SSTI state-space model is needed for obtaining a linearized small-signal model, as well as for calculating the equilibrium point where the model can be linearized.

In the context of Fig. 1, several different approaches for SSTI state-space representation of three-phase MMCs have

been recently proposed, with the aim of obtaining linearized models for small-signal power system stability analysis. A first approach has been to apply dynamic phasor modelling to all the internal electrical states of the MMC, as discussed in [16] and [17], resulting in complicated high order models. Another approach has been to neglect parts of the internal dynamics of the MMC, and model mainly the ac-side dynamics in a SRF together with a simplified dc-side representation, as in the models proposed in [18]-[20]. Among these studies, only the model from [19] includes a representation of the internal energy storage capacity of the sub-module capacitors and their dynamic impact on the power transfer between the ac and dc terminals. However, [19] did not derive any SSTI state-space representation that could be suitable for linearization. An approach based on further simplifications was applied in [18] and [20], assuming an ideal power balance between the ac- and dc-sides of the MMC in a similar way as for two-level VSCs. This implies significant inaccuracies in the model, since the transient responses of the internal variables and their controllers are not represented. Thus, such models are only suitable for studying slow dynamics.

To address these limitations, more detailed dynamic state space models have been proposed in [21]-[26]. Two different sets of assumptions and approximations are applied in the derivation of these publications:

i. The models presented in [21]-[24] assume that the MMC is operated with a Circulating Current Suppression Controller (CCSC) implemented in a negative sequence double frequency SRF, for eliminating the second harmonic components of the circulating current [27]. The different frequency components of the arm currents and the equivalent arm capacitor voltages are modelled by separate state-variables in their associated SRFs by applying phasor-based harmonic superposition. Thus, the couplings between the various frequency components are truncated as a first step of the model derivation. These models have revealed instability problems associated with interaction between the circulating currents, the internal capacitor voltages and the dc-side voltage as discussed in [22], [24]. However, the modelling approaches from [21]-[24] are not direcly suitable for representing MMCs with energy-based control strategies as will be explained in section II of this paper

ii. The approach presented in [25], [26] is based on a simplified representation of the MMC, where only the aggregated dynamics of the zero sequence circulating current and the total energy stored in the capacitors of the MMC are modelled. This approach is valid when the modulation indices for the MMC arms are calculated to compensate for the voltage oscillations in the internal equivalent arm capacitor voltages, as assumed in [6], [7], [28]. This modulation strategy will be referred to as Compensated Modulation (CM) and its implications for the modelling will be further elaborated in section II. These resulting models can accurately represent the external behaviour of the MMC at the ac-and dc-sides, but do not include the internal dynamics.

This paper demonstrates how an energy-based modelling approach inspired by [25]-[26] can capture also the internal current and energy dynamics of an MMC. The resulting model is derived from an average model with the sum and the difference of the arm energies in each phase as state variables and results in a complete and accurate SSTI representation of the MMC under the assumption of compensated modulation. Thus, the model covers a case that has not been previously studied in the available literature. Furthermore, the main contribution of the presented approach is that it inherently takes into account the coupling between the various frequency components of the MMC dynamics by a SSTI state-space representation. It is also shown how the detailed SSTI model can be simplified to the reduced order model from [25]-[26] by ignoring the states representing the oscillating components of the internal MMC variables. The validity of these two models are demonstrated by time-domain simulations in comparison to the SSTP nonlinear time-domain model of the MMC that was used as starting point for the model derivation. Finally, it is demonstrated how these state-space models can be linearized and utilized for analyzing the small-signal dynamics and control system tuning of the MMC by applying eigenvalue-based techniques.

II. MMC TOPOLOGY AND INSERTION INDEX CALCULATION

The model and the definitions that will be used as a starting point for deriving an MMC model with SSTI characteristics are briefly outlined in the following. This section also identifies how the derivations presented in this manuscript contributes to the SSTI representation of MMCs beyond what is available in previous literature.

A. Average Model of the Three-Phase Modular Multilevel Converter

The general topology of a three-phase MMC is shown in Fig. 2. In this case, operation in a cable-based HVDC transmission system is assumed, resulting in an equivalent capacitance C_{dc} at the dc terminals. The following nomenclature and conventions are applied for modelling of the MMC: italic lower case letters 'x' represent single variables, italic-bold letters '$\boldsymbol{x}$' represent vectors and matrices, whereas non-italic bold letters '$\mathbf{x}$' represent the complex space vector $\mathbf{x} = x_d + j \cdot x_q$.

With the above conventions, the main expressions associated with a generic phase $k \in a,b,c$ of an MMC are given by (1)-(5) [6].

$$i_{vk} = i_{uk} - i_{lk}, \qquad i_{ck} = \frac{i_{uk} + i_{lk}}{2} \tag{1}$$

$$v_{u,lk}^{\sigma} = \sum_{i=1}^{N} v_{u,lk}^{SM_i}, \qquad v_{u,lk} \approx n_{u,lk} \cdot v_{u,lk}^{\sigma} \tag{2}$$

$$e_{vk} = \frac{v_{lk} - v_{uk}}{2} \approx \frac{n_{lk} \cdot v_{lk}^{\sigma} - n_{uk} \cdot v_{uk}^{\sigma}}{2} \tag{3}$$

$$u_{ck} = \frac{v_{lk} + v_{uk}}{2} \approx \frac{n_{lk} \cdot v_{lk}^{\sigma} + n_{uk} \cdot v_{uk}^{\sigma}}{2} \tag{4}$$

$$w_{u,lk} \approx \frac{C_{SM}}{2N}\left(v_{u,lk}^{\sigma}\right)^2, \quad w_{\Sigma k} = w_{uk} + w_{lk}, \quad w_{\Delta k} = w_{uk} - w_{lk} \tag{5}$$

Assuming a fast capacitor voltage balancing algorithm, each arm output voltage $v_{u,lk}$ can be expressed by the product of the insertion index n resulting from a modulation algorithm and the sum arm capacitor voltage $v_{u,lk}^{\sigma}$, as expressed by the
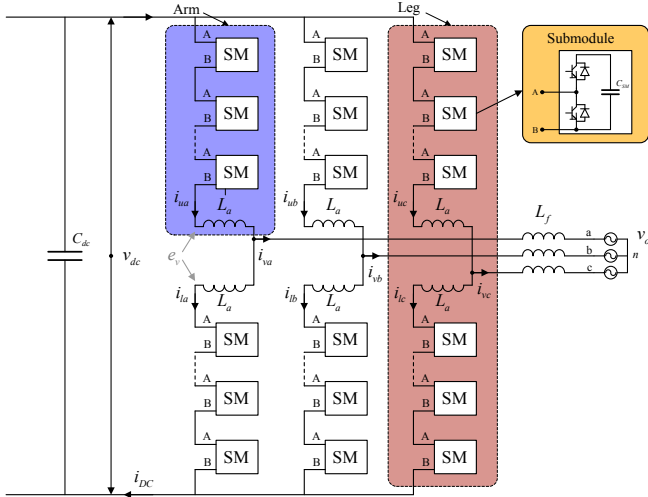
Fig. 2 Topology of a three-phase MMC

second part of (2) [7]. Thus, the voltage e_v, which drives the ac side currents from the MMC, can be expressed by (3). Similarly, the internal voltage of each leg u_c, which drives the circulating current, is defined as u_c and can be expressed by (4). The energy w stored in the capacitors of each arm is given by (5), which also defines the sum energy w_Σ and the energy difference w_Δ between the upper and lower arms [6], [7].

B. Calculation of insertion indexes: definition of compensated vs. un-compensated modulation

The specification of how the upper and lower arm insertion indexes are calculated is critical for the development of MMC models. A common approach for calculating the insertion indexes is given by [27], [30]:

$$n_u \approx \frac{-e_v^* + u_c^*}{V_{dc,nom}}, \qquad n_l \approx \frac{e_v^* + u_c^*}{V_{dc,nom}} \qquad (6)$$

Alternatively, the measured dc voltage v_{dc} can be used as the denominator in (6) [9], [13]. However, as long as the value in the denominator is constant during steady-state operation, the insertion index calculation according to (6) will not include any compensation for the continuous oscillations in the arm capacitor voltages. Thus, the influence of these oscillations will have to be compensated by the control loops. Such approaches for insertion index calculation can be referred to as "Un-Compensated Modulation" (UCM) [29].

This paper will consider the case when the insertion indexes are calculated by dividing the reference control voltages e_v^* and u_c^* by the measured or estimated time-varying aggregated voltage in the corresponding arm, $v_{u,l}^\sigma$ [6], [7]. As defined in [29], this approach will be referred as Compensated Modulation (CM) and can be expressed by:

$$n_u = \frac{-e_v^* + u_c^*}{v_u^\sigma}, \qquad n_l = \frac{e_v^* + u_c^*}{v_l^\sigma} \qquad (7)$$

With the CM approach, the division of the output of the controllers (i.e. $\pm e_v^* + u_c^*$) by $v_{u,l}^\sigma$ will compensate for the non-linearity caused by the product of the insertion indices and the time-periodic sum arm voltages in (3) and (4). Thus, it can be confirmed by substituting (7) into (3) and (4) that the voltages e_v and u_c that are driving the grid-side currents and the circulating currents respectively, will be equal to the voltage

reference outputs, e_v^* and u_c^*, of the corresponding controllers, as expressed by:

$$e_v = e_v^*; \qquad u_c = u_c^* \qquad (8)$$

As will be shown in the following sections, this characteristic is useful for deriving an energy-based SSTI representation of MMCs with CM-based control system implementations.

C. Selection of SSTI modelling approach according to insertion index calculation

It is demonstrated in [29] that energy-based models are not suitable for deriving SSTI representation of MMCs with UCM-based control, while voltage-based formulations are unsuitable for MMCs with CM-based control [29]. Indeed, voltage-based modelling approaches depending on harmonic superposition were applied for obtaining the SSTI representations and the corresponding linearized models of MMCs with UCM-based control in [17], [21]-[24]. The resulting models represent the internal dynamics of an MMC in *dqz*-variables associated with the SRFs corresponding to each oscillation frequency of the state variables in steady-state. An alternative voltage-based modelling approach for avoiding the approximations associated with harmonic superposition was proposed in [29].

In contrast to the voltage-based MMC models in [17], [21]-[24], simplified energy-based MMC models for the case of CM-based controls have been proposed in [25], [26]. However, no energy-based models with SSTI representation of the internal dynamics of the MMC in appropriate *dqz* reference frames are available in the literature.

An overview of how voltage-based or energy-based modelling approaches are suitable for deriving SSTI representations according to the selected strategy for insertion index calculation is shown in Fig. 3. As indicated in the figure, the main contribution of this paper is to fill a gap in the available literature by presenting the detailed derivation of an energy-based state-space model with SSTI representation of the internal dynamics of an MMC with CM-based control. Furthermore, it will be shown how simplification of the derived model results in the zero-sequence models from [25], [26].

III. MMC STATE-SPACE MODELLING FOR OBTAINING TIME-INVARIANCE IN STEADY-STATE

In the following subsections, a procedure for deriving a detailed energy-based SSTI representation of an MMC with CM-based control is presented. It is first shown how the average model in the stationary reference frame should be expressed to obtain separation of the dominant frequencies appearing in the MMC steady-state operation. On this basis, step-by-step derivations are presented for transforming the three-phase variables of the average model into a set of SRFs. The resulting model will inherently include the coupling between the different frequency components, even if all state-variables will settle to constant values in steady-state operation. Finally, it will be shown how the derived model can be simplified to the reduced order model of an MMC with CM-based control first presented in [25].

A. Mathematical derivation of a steady-state time-invariant MMC model based on energy formulation

To achieve SSTI characteristics without depending on harmonic superposition, the MMC variables should be
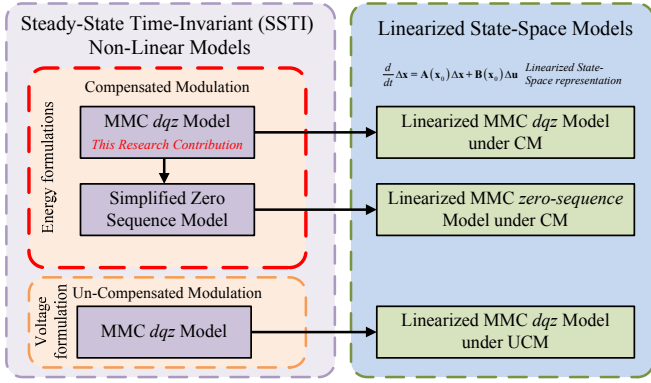
Fig. 3 Summary of relations between different models of MMCs with SSTI characteristics

expressed such that state variables associated with the different frequency components can be separated and transformed into their corresponding SRFs while retaining the coupling with variables associated with other frequency components. By choosing a $\sum$-Δ energy-based formulation according to (5) and considering the steady-state characteristics of the MMC according to [6], [7], the variables of the MMC can be separated into two groups, where each group is associated with a single frequency as:

$$-2\omega: \quad \boldsymbol{i}_c^{abc} = \boldsymbol{T}_{-2\omega}^{-1} \cdot \boldsymbol{i}_c^{dqz_{-2\omega}}; \quad \boldsymbol{u}_c^{abc} = \boldsymbol{T}_{-2\omega}^{-1} \cdot \boldsymbol{u}_c^{dqz_{-2\omega}}; \quad \boldsymbol{w}_\Sigma^{abc} = \boldsymbol{T}_{-2\omega}^{-1} \cdot \boldsymbol{w}_\Sigma^{dqz_{-2\omega}}$$
$$\omega: \quad \boldsymbol{i}_v^{abc} = \boldsymbol{T}_{+\omega}^{-1} \cdot \boldsymbol{i}_v^{dq_{+\omega}}; \quad \boldsymbol{e}_v^{abc} = \boldsymbol{T}_{+\omega}^{-1} \cdot \boldsymbol{e}_v^{dq_{+\omega}}; \quad \boldsymbol{w}_\Delta^{abc} = \boldsymbol{T}_{+\omega}^{-1} \cdot \boldsymbol{w}_\Delta^{dqz_{+\omega}} \quad (9)$$

Thus, the variables can be classified as those containing oscillations at -2ω ($\boldsymbol{i}_c$, $\boldsymbol{w}_\Sigma$ and $\boldsymbol{u}_c$), and those oscillating at $+\omega$ ($\boldsymbol{i}_v$, $\boldsymbol{w}_\Delta$ and $\boldsymbol{e}_v$). Furthermore, (9)shows how the stationary frame variables can be expressed from their equivalent SSTI dqz variables. The transformation matrixes $\boldsymbol{T}_\omega$ and $\boldsymbol{T}_{-2\omega}$ are representing the Park transformations, with phase angles synchronized with the grid voltage and its corresponding negative sequence double frequency, respectively.

The formulation of the MMC variables such that this initial separation of frequency components can be achieved constitutes the basis for the proposed modelling approach, as illustrated in Fig. 4. This figure indicates that Park transformations at different frequencies will be used to derive dynamic equations for equivalent *dqz* variables that are SSTI in their respective reference frames. In addition, a Park transformation $\boldsymbol{T}_{3\omega}$ at three times the grid frequency will be used to ensure a SSTI representation of the zero sequence of the energy difference, as will be discussed in subsection III.A.3). In the remainder of this section, the mathematical derivation of SSTI state equations representing the dynamics of a CM-controlled MMC will be described and expressed by using the definitions in (9) according to the approach illustrated by Fig. 4. Although the mathematical derivations involve several steps, the resulting model is relatively simple as summarized in section III.B. Similar procedures can also be applicable for obtaining SSTI characteristics of voltage-based MMC models for the case of UCM-based control, and for SSTI representation of stationary frame control systems.

1) Energy Sum dqz Dynamics

The dynamics of the energy sum $w_{\Sigma k}$ for a generic phase k can be expressed according to the definition introduced in [6]. When represented on vector form, the sum energy dynamics for the three phases are given by
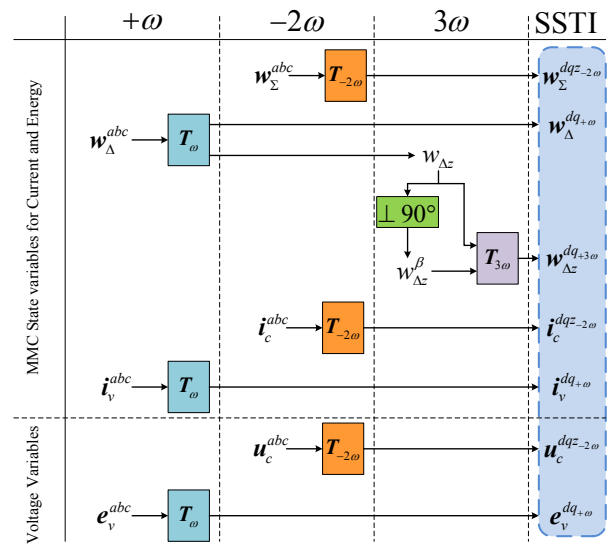

Fig. 4 The proposed modelling approach based on three Park transformations to achieve SSTI representation of MMC variables

$$\frac{d}{dt}\boldsymbol{w}_\Sigma^{abc} = -\boldsymbol{p}_v^{abc} + 2\boldsymbol{p}_c^{abc} \quad (10)$$

where $\boldsymbol{p}_v^{abc}$ and $\boldsymbol{p}_c^{abc}$ are the vectors defined in (11).

$$\boldsymbol{p}_v^{abc} = \begin{bmatrix} e_{va}i_{va} & e_{vb}i_{vb} & e_{vc}i_{vc} \end{bmatrix}^T$$
$$\boldsymbol{p}_c^{abc} = \begin{bmatrix} u_{ca}i_{ca} & u_{cb}i_{cb} & u_{cc}i_{cc} \end{bmatrix}^T \quad (11)$$

Since each component of the vector rows of $\boldsymbol{w}_\Sigma$, $\boldsymbol{p}_v$ and $\boldsymbol{p}_c$ oscillates at twice the fundamental grid frequency, (10) can be rewritten in a SRF at -2ω, as:

$$\frac{d}{dt}\boldsymbol{w}_\Sigma^{dqz_{-2\omega}} = -\boldsymbol{p}_v^{dqz_{-2\omega}} + 2\boldsymbol{p}_c^{dqz_{-2\omega}} + \boldsymbol{J}_{2\omega} \cdot \boldsymbol{w}_\Sigma^{dqz_{-2\omega}} \quad (12)$$

where $\boldsymbol{p}_v^{dqz_{-2\omega}}$ and $\boldsymbol{p}_c^{dqz_{-2\omega}}$ are expressed in (13) and (14) respectively. These equations show how the SRF variables are obtained from multiplication of the original vector in phase coordinates by the amplitude-invariant Park transformation matrix. Furthermore, $\boldsymbol{J}_{2\omega}$ is the cross-coupling matrix obtained by replacing $h=2$ in (15).

$$\boldsymbol{p}_v^{dqz_{-2\omega}} = \boldsymbol{T}_{-2\omega} \cdot \boldsymbol{p}_v^{abc} = \boldsymbol{T}_{-2\omega}\begin{bmatrix} e_{va}i_{va} & e_{vb}i_{vb} & e_{vc}i_{vc} \end{bmatrix}^T \quad (13)$$

$$\boldsymbol{p}_c^{dqz_{-2\omega}} = \boldsymbol{T}_{-2\omega} \cdot \boldsymbol{p}_c^{abc} = \boldsymbol{T}_{-2\omega}\begin{bmatrix} u_{ca}i_{ca} & u_{cb}i_{cb} & u_{cc}i_{cc} \end{bmatrix}^T \quad (14)$$

$$\boldsymbol{J}_{h\omega} \equiv \begin{bmatrix} 0 & h\cdot\omega & 0 \\ -h\cdot\omega & 0 & 0 \\ 0 & 0 & 0 \end{bmatrix}; \quad \forall h \in \mathbf{N}-\{0\} \quad (15)$$

The grid-side and circulating currents i_{vk} and i_{ck}, which appear in equations (13) and (14) along with the corresponding voltages e_{vk} and u_{ck}, can be expressed in their respective *dqz* rotating frames at $+\omega$ and -2ω by using the definitions given in (9). Hence, substituting the expressions for $\boldsymbol{e}_v^{abc}$ and $\boldsymbol{i}_v^{abc}$ resulting from (9) into equation (13), and solving the product between $\boldsymbol{T}_{-2\omega}$ and the resulting vector, yields in:

$$\boldsymbol{p}_v^{dqz_{-2\omega}} = \frac{1}{2}\begin{bmatrix} e_{vd_{+\omega}}i_{vd_{+\omega}} - e_{vq_{+\omega}}i_{vq_{+\omega}} \\ e_{vd_{+\omega}}i_{vq_{+\omega}} + e_{vq_{+\omega}}i_{vd_{+\omega}} \\ e_{vd_{+\omega}}i_{vd_{+\omega}} + e_{vq_{+\omega}}i_{vq_{+\omega}} \end{bmatrix} \quad (16)$$

Indeed, all variables in this expression will settle to a constant value in their associated SRF. Thus, (16) is a steady-state time-

invariant expression for the *dqz* components of the power flow from the grid-side of the MMC.

A similar procedure is repeated for $p_c^{dqz\text{-}2\omega}$ given in (14). Replacing each row of u_v^{abc} and i_c^{abc} as defined in (9) into (14), and expanding the multiplication with $T_{\text{-}2\omega}$ results in (17).

It is important to note that unlike (16), equation (17) contains a set of 6th order harmonic terms. However, the amplitudes of the 6th harmonic terms are all defined by products between *d*- and *q*-axis components of the circulating currents and the corresponding voltages. Since the amplitudes of u_c and i_c are small, the products between u_c and i_c will be very small compared to any of the terms containing a multiplication with the zero sequence voltage u_{cz} or the zero sequence current i_{cz}. Thus, these 6th order harmonic terms will have negligible influence on the power components defined by (17), and can be discarded to achieve time-invariance in steady state. It should be noted that this is the only approximation introduced in the derivations of the SSTI equations for representing the MMC, and that time-domain simulations confirm that this simplification is not compromising the accuracy of the model.

The energy sum dynamics in *dqz* coordinates can now be expressed by (18), where (16) and the first term of (17) have been substituted into (12).

$$\frac{d}{dt}w_\Sigma^{dqz\text{-}2\omega} = \frac{d}{dt}\begin{bmatrix} w_{\Sigma d_{\text{-}2\omega}} \\ w_{\Sigma q_{\text{-}2\omega}} \\ w_{\Sigma z} \end{bmatrix}$$

$$\approx \begin{bmatrix} -\frac{1}{2}\left(e_{vd_{+\omega}}i_{vd_{+\omega}} - e_{vq_{+\omega}}i_{vq_{+\omega}}\right) + 2\left(u_{cz}i_{cd_{\text{-}2\omega}} + u_{cd_{\text{-}2\omega}}i_{cz}\right) + 2\omega \cdot w_{\Sigma q_{\text{-}2\omega}} \\ -\frac{1}{2}\left(e_{vd_{+\omega}}i_{vq_{+\omega}} + e_{vq_{+\omega}}i_{vd_{+\omega}}\right) + 2\left(u_{cz}i_{cq_{\text{-}2\omega}} + u_{cq_{\text{-}2\omega}}i_{cz}\right) - 2\omega \cdot w_{\Sigma d_{\text{-}2\omega}} \\ -\frac{1}{2}\left(e_{vd_{+\omega}}i_{vd_{+\omega}} + e_{vq_{+\omega}}i_{vq_{+\omega}}\right) + u_{cd_{\text{-}2\omega}}i_{cd_{\text{-}2\omega}} + u_{cq_{\text{-}2\omega}}i_{cq_{\text{-}2\omega}} + 2u_{cz}i_{cz} \end{bmatrix} \quad (18)$$

Among these equations, the *dq* components, $w_{\Sigma,d,\text{-}2\omega}$ and $w_{\Sigma,q,\text{-}2\omega}$ represent the second harmonic oscillation superimposed to the average sum energy in the three phases. Indeed, when expressed as a space vector or on complex vector form (i.e. $\mathbf{w}_\Sigma^{dq,\text{-}2\omega} = w_{\Sigma,d,\text{-}2\omega} + j\,w_{\Sigma,q,\text{-}2\omega}$), these *dq*-components represent the three-phase second harmonic energy oscillations within the MMC. Thus, the amplitude of the sum energy oscillations and the phase angle with respect the reference frame orientation of the model (i.e. the phase angle detected by a Phase Locked Loop) is given by:

$$\left|w_\Sigma\right| = \sqrt{w_{\Sigma d}^2 + w_{\Sigma q}^2}, \qquad \varphi_{w_\Sigma} = \tan^{-1}\left(\frac{w_{\Sigma q}}{w_{\Sigma d}}\right) \quad (19)$$

The variable $w_{\Sigma z}$ represent the zero sequence component of the sum energy in the three phases, which is associated with the average value or dc-component of the total energy stored inside the MMC. Considering the relationships in (5), the different components of the sum energy can also be directly associated with the arm energies and the corresponding sum arm voltages.

2) Energy Difference dqz- Dynamics

The derivation of the steady-state time-invariant equations for the energy difference dynamics of the MMC is relatively similar to the case for the energy sum regarding its *dq*-components, yet very different regarding the zero-sequence. After presenting the first steps of the derivation, this section considers only the *dq*-dynamics, whereas the zero-sequence dynamics are addressed in the subsequent section.

As for the energy sum, the dynamic equation for the energy difference $w_{\Delta k}$ of a generic phase *k* is defined according to [6]. When expressed on vector form, the dynamics of the three phases are given by

$$\frac{d}{dt}w_\Delta^{abc} = p_{\Delta 1}^{abc} + p_{\Delta 2}^{abc} \quad (20)$$

where $p_{\Delta 1}^{abc}$ and $p_{\Delta 2}^{abc}$ are defined by

$$p_{\Delta 1}^{abc} = -2\begin{bmatrix} e_{va}i_{ca} & e_{vb}i_{cb} & e_{vc}i_{cc} \end{bmatrix}^T$$
$$p_{\Delta 2}^{abc} = \begin{bmatrix} u_{ca}i_{va} & u_{cb}i_{vb} & u_{cc}i_{vc} \end{bmatrix}^T \quad (21)$$

Since the main frequency component of the energy difference dynamics in steady state is the fundamental frequency of the grid voltage, (20) can be re-written in the SRF rotating at $+\omega$, yielding in

$$\frac{d}{dt}w_\Delta^{dqz+\omega} = p_{\Delta 1}^{dqz+\omega} + p_{\Delta 2}^{dqz+\omega} + J_\omega \cdot w_\Delta^{dqz+\omega} \quad (22)$$

where $p_{\Delta 1}^{dqz+\omega}$ and $p_{\Delta 2}^{dqz+\omega}$ are expressed in (23) and (24) respectively. These equations are obtained by multiplying the original vector in the stationary *abc* reference frame by the Park transformation matrix at $+\omega$; i.e., $T_{+\omega}$.

$$p_{\Delta 1}^{dqz+\omega} = T_{+\omega} \cdot p_{\Delta 1}^{abc} = -2T_{+\omega}\begin{bmatrix} e_{va}i_{ca} & e_{vb}i_{cb} & e_{vc}i_{cc} \end{bmatrix}^T \quad (23)$$

$$p_{\Delta 2}^{dqz+\omega} = T_{+\omega} \cdot p_{\Delta 2}^{abc} = T_{+\omega}\begin{bmatrix} u_{ca}i_{va} & u_{cb}i_{vb} & u_{cc}i_{vc} \end{bmatrix}^T \quad (24)$$

Substituting into (23) the expressions for the voltage e_v^{abc} and the circulating current i_c^{abc} that can be obtained from the definitions given in (9), the individual elements of $p_{\Delta 1}^{dqz+\omega}$ can be expressed as a function of the *dqz* current and voltage components:

$$p_{\Delta 1}^{dqz+\omega} = -\begin{bmatrix} e_{vd_{+\omega}}i_{cd_{\text{-}2\omega}} + e_{vq_{+\omega}}i_{cq_{\text{-}2\omega}} + 2e_{vd_{+\omega}}i_{cz} \\ e_{vd_{+\omega}}i_{cq_{\text{-}2\omega}} - e_{vq_{+\omega}}i_{cd_{\text{-}2\omega}} + 2e_{vq_{+\omega}}i_{cz} \\ \left(e_{vd_{+\omega}}i_{cd_{\text{-}2\omega}} - e_{vq_{+\omega}}i_{cq_{\text{-}2\omega}}\right)\cos\left(3\omega t\right)... \\ ...-\left(e_{vd_{+\omega}}i_{cq_{\text{-}2\omega}} + e_{vq_{+\omega}}i_{cd_{\text{-}2\omega}}\right)\sin\left(3\omega t\right) \end{bmatrix} \quad (25)$$

Contrary to the power expressions given in (16), (17) only the *d*- and *q*-axis components of (25) are time-invariant in steady state. Indeed, the zero-sequence component $p_{\Delta 1z}$ given in (25) is time-periodic, with third harmonic oscillations in steady state. The origin of this third harmonic component is the multiplication of variables containing fundamental frequency and double frequency components. Indeed, the zero sequence component of (25) shows that the amplitude of the third harmonic oscillations depends on products between the circulating currents and the ac-side voltage. Thus, they cannot be neglected in a detailed model of the MMC.

Similarly as for $p_{\Delta 1}^{dqz+\omega}$, it is possible to express $p_{\Delta 2}^{dqz+\omega}$ as a

$$p_c^{dqz\text{-}2\omega} = \begin{bmatrix} u_{cz}i_{cd_{\text{-}2\omega}} + u_{cd_{\text{-}2\omega}}i_{cz} \\ u_{cz}i_{cq_{\text{-}2\omega}} + u_{cq_{\text{-}2\omega}}i_{cz} \\ \frac{1}{2}u_{cd_{\text{-}2\omega}}i_{cd_{\text{-}2\omega}} + \frac{1}{2}u_{cq_{\text{-}2\omega}}i_{cq_{\text{-}2\omega}} + u_{cz}i_{cz} \end{bmatrix} + \underbrace{\begin{bmatrix} +\frac{1}{2}\left(u_{cd_{\text{-}2\omega}}i_{cd_{\text{-}2\omega}} - u_{cq_{\text{-}2\omega}}i_{cq_{\text{-}2\omega}}\right)\cos(6\omega t) - \frac{1}{2}\left(u_{cq_{\text{-}2\omega}}i_{cd_{\text{-}2\omega}} - u_{cd_{\text{-}2\omega}}i_{cq_{\text{-}2\omega}}\right)\sin(6\omega t) \\ -\frac{1}{2}\left(u_{cd_{\text{-}2\omega}}i_{cd_{\text{-}2\omega}} - u_{cq_{\text{-}2\omega}}i_{cq_{\text{-}2\omega}}\right)\sin(6\omega t) - \frac{1}{2}\left(u_{cq_{\text{-}2\omega}}i_{cd_{\text{-}2\omega}} + u_{cd_{\text{-}2\omega}}i_{cq_{\text{-}2\omega}}\right)\cos(6\omega t) \\ 0 \end{bmatrix}}_{\approx 0} \quad (17)$$

function of *dqz* currents and voltages. This is obtained by replacing the expressions for $\boldsymbol{i}_v^{abc}$ and $\boldsymbol{u}_c^{abc}$ according to (9), into (24). By solving for the individual elements of $\boldsymbol{p}_{\Delta 2}^{dqz+\omega}$, (24) can be expressed as a function of the *dqz* current and voltage components, as given by

$$\boldsymbol{p}_{\Delta 2}^{dqz+\omega} = \begin{bmatrix} \left(\tfrac{1}{2}u_{cd_{-2\omega}}+u_{cz}\right)i_{vd_{+\omega}}+\tfrac{1}{2}u_{cq_{-2\omega}}i_{vq_{+\omega}} \\ \tfrac{1}{2}u_{cq_{-2\omega}}i_{vd_{+\omega}}+\left(-\tfrac{1}{2}u_{cd_{-2\omega}}+u_{cz}\right)i_{vq_{+\omega}} \\ \tfrac{1}{2}\left(u_{cd_{-2\omega}}i_{vd_{+\omega}}-u_{cq_{-2\omega}}i_{vq_{+\omega}}\right)\cos\left(3\omega t\right)... \\ ...-\tfrac{1}{2}\left(u_{cq_{-2\omega}}i_{vd_{+\omega}}+u_{cd_{-2\omega}}i_{vq_{+\omega}}\right)\sin\left(3\omega t\right) \end{bmatrix} \quad (26)$$

As for $p_{\Delta 1z}$, the zero-sequence component $p_{\Delta 2z}$, expressed in (26), is not time-invariant in steady state. Thus, the zero sequence components in (25) and (26) will be further analyzed in the following sub-section.

Considering only the *d*- and *q*-axis components of the power vectors from (25) and (26), and substituting the obtained expressions into (22) results in the dynamic equations for the *d*- and *q*-axis energy difference as expressed by (27).

These two state equations do not require any further simplifications since all their elements are already SSTI. Indeed, $w_{\Delta,d,+\omega}$ and $w_{\Delta,q,+\omega}$ represent the fundamental frequency oscillations of the energy difference between the upper and the lower arms of the MMC. Thus, the amplitude and phase angle of these oscillations is accurately represented by the energy difference *dq* components (i.e. $\boldsymbol{w}_\Delta^{dq,+\omega} = w_{\Delta,d,+\omega} + j\, w_{\Delta,q,+\omega}$). Based on (5), it can also be understood how these signals are directly associated to the fundamental frequency oscillation in the sum arm energies and the corresponding variations in the sum arm voltages.

3) The energy difference zero-sequence dynamics

Since the zero sequence components in (25) and (26) are time-periodic in steady state, further reformulation is necessary to obtain a SSTI representation of the zero sequence energy difference dynamics of the MMC. This can be obtained by defining a virtual signal $w_{\Delta z}^\beta$ which is 90° shifted with respect to the original "single-phase" time-periodic zero sequence energy difference signal $w_{\Delta z}$ given in (26). This approach is conceptually similar to the commonly applied strategy of generating a virtual two-phase system for representing single-phase systems in a SRF [31]. However, since the amplitudes of the different sine and cosine components are defined by SSTI variables, the signal $w_{\Delta z}^\beta$ can be identified within the model, and without causing any additional delay. The actual and virtual energy difference zero-sequence variables can be labelled as $w_{\Delta z}^\alpha$ and $w_{\Delta z}^\beta$ and together they define an orthogonal $\alpha\beta$-system. This $\alpha\beta$ system can be expressed by (28), with $p_{\Delta 1z}^\alpha$ and $p_{\Delta 2z}^\alpha$ defined by (25) and (26), whereas $p_{\Delta 1z}^\beta$ and $p_{\Delta 2z}^\beta$ are created by replacing the "cos(*3ωt*)" and "sin(*3ωt*)" terms that

appear in the α-signal by "−sin(*3ωt*)" and "cos(*3ωt*)," respectively. Thus, the amplitude of the β-signals will be identical to the α-signal amplitude.

$$\frac{d}{dt}\boldsymbol{w}_{\Delta z}^{\alpha\beta} = \boldsymbol{p}_{\Delta 1z}^{\alpha\beta} + \boldsymbol{p}_{\Delta 2z}^{\alpha\beta} \quad (28)$$

This orthogonal system can be represented by variables defined in a SRF at 3ω. Hence, the αβ-vectors on the right hand side of (28) can be expressed by (29), where $p^{d3\omega}{}_{\Delta 1z}$, $p^{q3\omega}{}_{\Delta 1z}$, $p^{d3\omega}{}_{\Delta 2z}$ and $p^{q3\omega}{}_{\Delta 2z}$, are defined by (30).

$$\boldsymbol{p}_{\Delta 1z}^{\alpha\beta} = \begin{bmatrix} p_{\Delta 1z}^\alpha & p_{\Delta 1z}^\beta \end{bmatrix}^T = \boldsymbol{T}_{+3\omega}^{-1}\cdot\begin{bmatrix} p_{\Delta 1z}^{d+3\omega} & p_{\Delta 1z}^{q+3\omega} \end{bmatrix}^T = \boldsymbol{T}_{+3\omega}^{-1}\cdot\boldsymbol{p}_{\Delta 1z}^{dq+3\omega},$$
$$\boldsymbol{p}_{\Delta 2z}^{\alpha\beta} = \begin{bmatrix} p_{\Delta 2z}^\alpha & p_{\Delta 2z}^\beta \end{bmatrix}^T = \boldsymbol{T}_{+3\omega}^{-1}\cdot\begin{bmatrix} p_{\Delta 2z}^{d+3\omega} & p_{\Delta 2z}^{q+3\omega} \end{bmatrix}^T = \boldsymbol{T}_{+3\omega}^{-1}\cdot\boldsymbol{p}_{\Delta 2z}^{dq+3\omega} \quad (29)$$

$$p_{\Delta 1z}^{d+3\omega} = -\left(e_{vd_{+\omega}}i_{cd_{-2\omega}}-e_{vq_{+\omega}}i_{cq_{-2\omega}}\right); \quad p_{\Delta 2z}^{d+3\omega} = \tfrac{1}{2}\left(u_{cd_{-2\omega}}i_{vd_{+\omega}}-u_{cq_{-2\omega}}i_{vq_{+\omega}}\right)$$
$$p_{\Delta 1z}^{q+3\omega} = -\left(e_{vd_{+\omega}}i_{cq_{-2\omega}}+e_{vq_{+\omega}}i_{cd_{-2\omega}}\right); \quad p_{\Delta 2z}^{q+3\omega} = \tfrac{1}{2}\left(u_{cq_{-2\omega}}i_{vd_{+\omega}}+u_{cd_{-2\omega}}i_{vq_{+\omega}}\right) \quad (30)$$

The dynamics of the energy difference zero-sequence αβ vector $w_{\Delta z}^{\alpha\beta}$ from (28) can be transformed into the rotating *dq*-reference frame at +3ω by means of $\boldsymbol{T}_{+3\omega}$ and the definitions given in (29)-(30), yielding in:

$$\frac{d}{dt}\boldsymbol{w}_{\Delta z}^{dq+3\omega} = \boldsymbol{p}_{\Delta 1z}^{dq+3\omega} + \boldsymbol{p}_{\Delta 2z}^{dq+3\omega} + \boldsymbol{J}_{3\omega}\cdot\boldsymbol{w}_{\Delta z}^{dq+3\omega} \quad (31)$$

Introducing the power definitions in (30), (31) can be expressed by (32).

It is possible to confirm by simple inspection that the zero-sequence dynamics of the energy difference expressed in the form of (32) are SSTI as long as the *d*- and *q*-axis components of e_v, u_c, i_v and i_c in their associated SRFs are SSTI. Therefore, this equation preserves time-invariance when the circulating current is controlled to inject a 2nd harmonic component (for energy shaping) as well as for suppression of the 2nd harmonic circulating current according to [27].

When considering the zero sequence energy difference dynamics in (32), it should be kept in mind that this is a orthogonal vector representation of a single phase sinusoidal signal. Indeed, since the third harmonic oscillation is a zero sequence component, the same signal appears in all the three phases of the MMC. The amplitude of this signal and the phase angle with respect to the third harmonic SRF can be found directly from the vector amplitude and phase angle of the defined *dq* zero sequence energy variables (i.e. $\boldsymbol{w}_{\Delta z}^{dq,+3\omega} = w_{\Delta z}^{d,+3\omega} + j\,w_{\Delta z}^{q,+3\omega}$). It can also be understood from (5) how these third harmonic oscillations will appear in the sum arm energies and in the corresponding sum arm voltages.

4) Circulating current dynamics

The dynamics of the circulating currents are recalled in (33) in vector representation for a three-phase MMC [7].

$$L_a\frac{d}{dt}\boldsymbol{i}_c^{abc} = -R_a\cdot\boldsymbol{i}_c^{abc} - \boldsymbol{u}_c^{abc} + \frac{v_{dc}}{2}\begin{bmatrix} 1 & 1 & 1 \end{bmatrix}^T \quad (33)$$

Equation (33) can be easily expressed in the SRF rotating at −2ω, yielding in (34).

$$\frac{d}{dt}\boldsymbol{w}_\Delta^{dq+\omega} = \frac{d}{dt}\begin{bmatrix} w_{\Delta d_{+\omega}} \\ w_{\Delta q_{+\omega}} \end{bmatrix} = \begin{bmatrix} -\left(e_{vd_{+\omega}}i_{cd_{-2\omega}}+e_{vq_{+\omega}}i_{cq_{-2\omega}}+2e_{vd_{+\omega}}i_{cz}\right) \\ -\left(e_{vd_{+\omega}}i_{cq_{-2\omega}}-e_{vq_{+\omega}}i_{cd_{-2\omega}}+2e_{vq_{+\omega}}i_{cz}\right) \end{bmatrix} + \begin{bmatrix} \left(\tfrac{1}{2}u_{cd_{-2\omega}}+u_{cz}\right)i_{vd_{+\omega}}+\tfrac{1}{2}u_{cq_{-2\omega}}i_{vq_{+\omega}}+\omega\cdot w_{\Delta q_{+\omega}} \\ \tfrac{1}{2}u_{cq_{-2\omega}}i_{vd_{+\omega}}+\left(-\tfrac{1}{2}u_{cd_{-2\omega}}+u_{cz}\right)i_{vq_{+\omega}}-\omega\cdot w_{\Delta d_{+\omega}} \end{bmatrix} \quad (27)$$

$$\frac{d}{dt}\boldsymbol{w}_{\Delta z}^{dq+3\omega} = \frac{d}{dt}\begin{bmatrix} w_{\Delta z}^{d+3\omega} \\ w_{\Delta z}^{q+3\omega} \end{bmatrix} = \begin{bmatrix} -\left(e_{vd_{+\omega}}i_{cd_{-2\omega}}-e_{vq_{+\omega}}i_{cq_{-2\omega}}\right)+\tfrac{1}{2}\left(u_{cd_{-2\omega}}i_{vd_{+\omega}}-u_{cq_{-2\omega}}i_{vq_{+\omega}}\right)+3\omega\cdot w_{\Delta z}^{q+3\omega} \\ -\left(e_{vd_{+\omega}}i_{cq_{-2\omega}}+e_{vq_{+\omega}}i_{cd_{-2\omega}}\right)+\tfrac{1}{2}\left(u_{cq_{-2\omega}}i_{vd_{+\omega}}+u_{cd_{-2\omega}}i_{vq_{+\omega}}\right)-3\omega\cdot w_{\Delta z}^{d+3\omega} \end{bmatrix} \quad (32)$$

$$\frac{d}{dt}\mathbf{i}_c^{dqz-2\omega} = \left(-\frac{R_a}{L_a}\mathbf{I} + \mathbf{J}_{2\omega}\right)\mathbf{i}_c^{dqz-2\omega} - \frac{1}{L_a}\mathbf{u}_c^{dqz-2\omega} + \frac{v_{dc}}{2L_a}[0 \quad 0 \quad 1]^T \quad (34)$$

The equations for the *dq*-components of the circulating currents have the same form as for any SRF representation of currents in a three phase system. However, the zero sequence component is a dc-signal, representing the dc-component of the circulating currents of the three phases and is directly associated to the power transfer between the ac- and dc-sides of the MMC.

B. Summary of derived model with SSTI representation of MMC internal dynamics

The individual equations describing the internal dynamics of the MMC as represented by SSTI state variables, as derived in the previous subsections, are summarized here. The resulting SSTI state equations are collected in (35) and result directly from (18), (27), (32) and (34) by expressing the *dq*-components with complex vector notation. The algebraic equations linking the controller outputs, u_c^* and e_v^*, with the rest of the system are given by (36).

$$\frac{d}{dt}\mathbf{w}_\Sigma^{dq-2\omega} = -\frac{1}{2}\mathbf{e}_v^{dq+\omega}\mathbf{i}_v^{dq+\omega} + 2\left(u_{cz}\mathbf{i}_c^{dq-2\omega} + \mathbf{u}_c^{dq-2\omega}i_{cz}\right) - j\cdot2\omega\mathbf{w}_\Sigma^{dq-2\omega}$$

$$\frac{d}{dt}w_{\Sigma z} = -\frac{1}{2}\mathrm{Re}\left\{\overline{\mathbf{e}}_v^{dq+\omega}\mathbf{i}_v^{dq+\omega}\right\} + \mathrm{Re}\left\{\overline{\mathbf{u}}_c^{dq-2\omega}\mathbf{i}_c^{dq-2\omega}\right\} + 2u_{cz}i_{cz}$$

$$\frac{d}{dt}\mathbf{w}_\Delta^{dq+\omega} = -\overline{\mathbf{e}}_v^{dq+\omega}\mathbf{i}_c^{dq-2\omega} + 2\mathbf{e}_v^{dq+\omega}i_{cz} + \frac{1}{2}\mathbf{u}_c^{dq-2\omega}\overline{\mathbf{i}}_v^{dq+\omega} + u_{cz}\mathbf{i}_v^{dq+\omega} - j\cdot\omega\mathbf{w}_\Delta^{dq+\omega}$$

$$\frac{d}{dt}\mathbf{w}_{\Delta z}^{dq+3\omega} = -\mathbf{e}_v^{dq+\omega}\mathbf{i}_c^{dq-2\omega} + \frac{1}{2}\mathbf{u}_c^{dq-2\omega}\mathbf{i}_v^{dq+\omega} - j\cdot3\omega\mathbf{w}_{\Delta z}^{dq+3\omega}$$

$$\frac{d}{dt}\mathbf{i}_c^{dq-2\omega} = -\left(\frac{R_a}{L_a} + j\cdot2\omega\right)\mathbf{i}_c^{dq-2\omega} - \frac{1}{L_a}\mathbf{u}_c^{dq-2\omega}$$

$$\frac{d}{dt}i_{cz} = -\frac{R_a}{L_a}i_{cz} + \frac{1}{L_a}\cdot\frac{v_{dc}}{2} - \frac{1}{L_a}\cdot u_{cz}$$

$$(35)$$

$$\mathbf{u}_c^{dq-2\omega} = \mathbf{u}_c^{*,dq-2\omega}; \quad u_{cz} = u_{cz}^*; \quad \mathbf{e}_v^{dq+\omega} = \mathbf{e}_v^{*,dq+\omega} \quad (36)$$

These equations define a non-linear SSTI state-space representation of the average model of an MMC with energy-based formulation according to [6], [7]. The only simplification introduced during the derivation is that the 6th harmonic terms in (17) have been neglected. Thus, the developed SSTI equations preserve the dynamics and the non-linear relationships of the model it is derived from, and inherits the same limitations as the analytical average models in the stationary frame. As for any other analytical average model, this implies that the developed SSTI representation of the MMC is not representing any physical saturation limits within the model, like for instance the over-modulation limit that can be reached if the voltage reference for the converter is higher than the available voltage in the internal capacitors. However, as long as the converter is operated within its limitations, the derived model is containing detailed information about the dynamic characteristics as well as the steady-state operating conditions of the MMC. Thus, the model inherently includes the dynamic coupling between the various frequency components, which can be clearly noticed by considering that several of the state equations in (35) are defined by *dq* variables from SRFs at different frequencies.

It should also be noted that the model in (35) effectively represents the MMC by 10 SSTI state-equations. The grid-side currents are not included in these equations, as they contains only a fundamental frequency component and can be directly modelled in the SRF at the fundamental frequency. Considering the MMC topology from Fig. 2, representation of the 6 equivalent arm capacitor voltages and the 3 circulating currents as state-variables will imply a model with 9 states. Thus, the derived SSTI representation of the MMC includes only one additional state equation, since two state variables are required to obtain a SSTI representation of the zero sequence energy difference, $w_{\Delta z}$.

C. Simplified zero-sequence model of MMC

Observing the structure of the model in (35), it can be noticed that the dynamics of the zero sequence current i_{cz} do not depend on any of the *dq*-variables. Furthermore, the dynamic equation for the zero sequence sum energy $w_{\Sigma z}$ contains terms depending on the product of the *dq*-components of $\mathbf{u}_c$ and $\mathbf{i}_c$. Since the *dq*-components of $\mathbf{u}_c$ are significantly smaller than the zero sequence component, u_{cz}, and the amplitude of the ac-side voltages, $\mathbf{e}_v$, the influence of these terms on the sum energy dynamics will be very small. Under the assumption of compensated modulation, this implies that a simplified model for representing only the zero-sequence component of the MMC internal variables can be obtained, as given by (37).

$$\frac{d}{dt}w_{\Sigma z} \approx -\frac{1}{2}\left(e_{vd_{+\omega}}i_{vd_{+\omega}} + e_{vq_{+\omega}}i_{vq_{+\omega}}\right) + 2u_{cz}i_{cz}$$

$$\frac{d}{dt}i_{cz} = -\frac{R}{L}i_{cz} - \frac{1}{L}u_{cz}^* + \frac{1}{2L}v_{dc}$$

$$(37)$$

This simplification and reduction of the equations from (35) is directly resulting in the model proposed by [25], [26]. It can also be understood from the structure of the detailed model in (35) that the simplified model in (37) will be suitable as a "macroscopic" model of the ac- and dc-side dynamics of the MMC by considering only the zero sequence components of the energy-sum and the circulating current. Thus, the derivation of the detailed model provides a theoretical basis for verifying the accuracy and for understanding the level of approximation implied by the simplified models in [25], [26].

The zero-sequence-based reduced order MMC model in (37) has a lower number of equations and is much simpler to implement than the detailed model in (35). However, it will be verified that under CM-based control, the zero-sequence model is accurately representing the dynamics of the states that influence the external behaviour at the ac- and dc-sides (i.e. v_{dc}, u_{cz}, i_{cz}, $w_{\Sigma z}$, $\mathbf{e}_v^{dq}$ and $\mathbf{i}_v^{dq}$). Indeed, these variables remain practically unaffected by the dynamics of the neglected internal variables ($\mathbf{w}_\Sigma^{dq}$, $\mathbf{w}_\Delta^{dqz}$, $\mathbf{i}_c^{dq}$ and $\mathbf{u}_c^{dq}$) as long as their dynamics are stable and the insertion indexes are calculated according to (6). Thus, the zero-sequence model only preserves information about the power balance between the ac-side, the internally stored energy and the dc-terminals. Hence, it is expected that this zero-sequence model will be of most interest for large-scale power system stability studies, when the internal dynamics of the MMC are of limited interest.
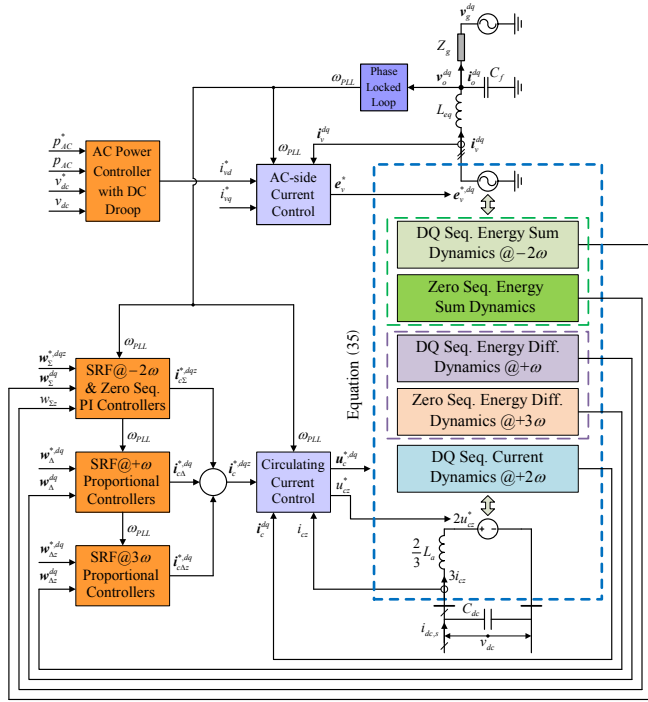
Fig. 5 Overview of the derived time-invariant MMC model with representation of the internal *dqz* dynamics, including ac-side and dc-side dynamics as well as all elements of the applied control system

IV. SIMPLIFIED CONTROL SYSTEM FOR SSTI REPRESENTATION

The MMC model under CM cannot be tested or validated without introducing a closed loop control scheme. Therefore, this section briefly introduces a simplified closed loop control system adapted to the SSTI representation. Note that the purpose of the added controllers is to enable comparison of the derived SSTI representation with an established MMC average model, without requiring significant efforts in modelling of the control system.

An overview of the entire model of an MMC HVDC terminal, including the control loops as well as the ac- and dc-side electrical dynamics is shown in Fig. 5. Conventional SRF PI current controllers with decoupling terms are applied for controlling the ac-side currents of the MMC [25], [32]. An ac-side PI power controller, based on feedback of a low-pass-filtered measurement of the power flowing from the MMC into the grid, is providing the d-axis active current reference to the current controllers. However, a dc voltage droop function based on a low-pass-filtered measurement of the voltage at the dc terminals is acting on the active power reference. For simplicity, the q-axis current reference is kept equal to zero. Furthermore, a SRF Phase Locked Loop (PLL) is utilized to synchronize the control system of the MMC to the measured grid voltage v_o. The state equations for the ac-side controllers of a three-phase VSC, the dc voltage droop function and the PLL from [25] and [32] can be utilized for state-space representation of the system without modifications.

The zero sequence components of the circulating current and the sum energy are controlled by PI controllers, utilizing the same equations as in [25]. Furthermore, a set of decoupled

SRF PI controllers in the double frequency negative sequence reference frame, according to [27], controls the *dq*-components of the circulating currents. An identical PI-controller structure with energy decoupling terms at $2\omega_{PLL}$ regulates the *dq*-components of the sum energy, by providing current references for the circulating current controllers. Furthermore, a simple proportional controller with decoupling terms at ω_{PLL} regulates the energy difference *dq*-component dynamics. Similarly, the *dq*-components of the zero sequence of the energy difference are controlled by an additional proportional controller with decoupling terms at $3\omega_{PLL}$. The contribution of each energy controller is added to form the reference for the circulating current as illustrated in Fig. 5.

It should be noted that the derived MMC model could be combined with different control system implementations. However, accurate SSTI representation of commonly applied control loops implemented in the stationary reference frame would require similar derivations as presented for the MMC topology. Such derivations and subsequent analysis are beyond the scope of this manuscript, but an example of how an SSTI representation of stationary frame per-phase energy-based control strategies can be obtained is presented in [34].

V. MODELS OF MMCS INCLUDING AC-SIDE AND DC-SIDE GRID DYNAMICS

By combining the SSTI state-space representation of the MMC dynamics derived in section III.A with the simplified control structure introduced in section IV, it is possible to establish state space models of an MMC integrated into any ac- or dc grid configuration. For simplicity, only the configuration from Fig. 5 will be studied here, although the derived models can be directly utilized for studies of larger system configurations, for instance in point-to-point or multi-terminal HVDC transmission schemes by similar approaches as discussed in [35], [36].

A. MMC models with ac-side and dc-side grid dynamics

The equations of the ac-side dynamics included in the model result directly from the circuit diagram indicated in Fig. 5, the average modelling of each arm of the MMC topology and the assumption of CM-based control [6], [7], [12], [33]. Thus, the ac-side model represented in the SRF is the same as for a 2-L VSC, and the same approach as in [25], [32] can be applied for obtaining a SSTI state-space representation including the PLL dynamics.

The dc-side is modelled with a capacitor representing the equivalent capacitance of an HVDC cable, and a current source $i_{dc,s}$ representing the cable current, as shown in Fig. 2. Thus, the electrical dynamics at the dc terminals can be modelled by the same equations as in [25].

B. Non-linear state-space models with SSTI solution

A general SSTI state-space model of the studied system can be expressed on standard form according to [15], [14]:

$$\dot{x} = f(x, u), \quad y = g(x, u) \qquad (38)$$

Models including the detailed MMC dynamics according to (35) and Fig. 5, as well as models based on the simplified zero-sequence representation of the MMC from (37) can be easily developed on the same form.
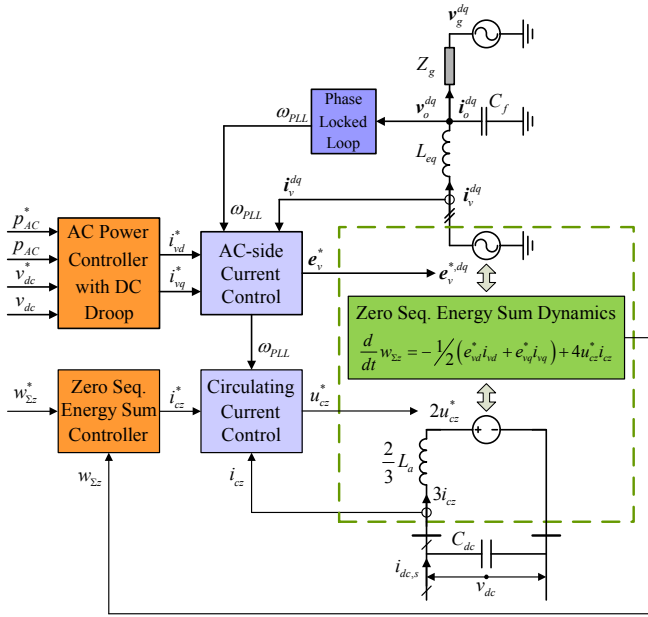
Fig. 6 Overview of the simplified time-invariant MMC model

1) Model with detailed representation of MMC

Based on all presented derivations and references, a SSTI representation of the entire system from Fig. 5 can be represented by the state vector x and the input vector u as defined by (39) and (40), respectively.

Thus, the SSTI state space representation including ac- and dc-side interfaces, as well as the grid synchronization dynamics on the ac-side results in a model with 34 states and 13 input variables. In addition to the state variables already explained, the states γ and φ are associated to the ac-side current control, while all variables with subscript 'PLL' are associated to the Phase Locked Loop used for grid synchronization, as described in detail in [32]. The low-pass filtered dc voltage is given by $v_{dc,f}$, the low-pass filtered measurement of the ac-side power flow is defined by the state $p_{ac,m}$, and ρ defines the integrator state of the PI-controller for the ac-side power flow. The states κ are integrator states of the PI controllers regulating the sum energy components, while ξ defines the PI controller states for the d- q- and z-components of the circulating currents.

2) Simplified zero-sequence MMC Model

A non-linear SSTI state-space model including a representation of the MMC by the simplified zero sequence representation from (37) [25], [26], can be established in the same way as for the detailed model. The only difference will be that the states $w_{\Sigma d}$, $w_{\Sigma q}$, $w_{\Delta d}$, $w_{\Delta q}$, $w_{\Delta zd}$, $w_{\Delta zq}$, $\kappa_{\Sigma d}$, $\kappa_{\Sigma q}$ ξ_d and ξ_q as well as the input signals $w^*_{\Sigma,d}$, $w^*_{\Sigma,q}$, $w^*_{\Delta,d}$, $w^*_{\Delta,q}$, $w^*_{\Delta z,d}$ and $w^*_{\Delta z,q}$ will be eliminated. Thus, with the simplified MMC representation, the structure of the model will be reduced to the simplified configuration shown in Fig. 6.

C. Linearized small-signal models

As mentioned, the need for obtaining a linearized state-

space model for conducting eigenvalue-based studies of small-signal stability is among the main motivations for deriving a SSTI representation of the MMC. However, a non-linear SSTI representation in the form of (38) is also necessary for calculating the steady-state operating point. Thus, any feasible steady-state operating condition of the system can be found by solving for the values of the state variables when imposing $\dot{x} = 0$. Subsequently, the model can be linearized at the selected steady-state operating point. For a generic linearization point x_0, the linearized small-signal state-space model can be obtained by considering the first order derivatives with respect to all state variables and input signals [14], [15], and can be expressed as:

$$\Delta\dot{x} = \mathbf{A}(x_0) \cdot \Delta x + \mathbf{B}(x_0) \cdot \Delta u$$
$$\Delta y = \mathbf{C}(x_0) \cdot \Delta x + \mathbf{D}(x_0) \cdot \Delta u \quad (41).$$

where the prefix Δ denotes small-signal deviations around the steady-state operating point.

VI. MODEL VALIDATION BY TIME-DOMAIN SIMULATION

To validate the derived SSTI equations, the detailed as well as the simplified representation of the MMC, and the corresponding small-signal models, results from time-domain simulation of five different models will be shown and discussed in this section. These models correspond to the following cases:

1) The reference case is a circuit-based average model of a three-phase MMC, where each arm is represented by a controlled voltage source and where the internal arm voltage dynamics are represented by an equivalent arm capacitance as shown in Fig. 7 [7], [12] [33]. This model includes nonlinear effects, except for the switching operations and the dynamics of the sub-module capacitor voltage balancing algorithms. Since this model is well-established for analysis and simulation of MMCs, and has been previously verified by laboratory-scale experiments in [7], [12], it will be used as a benchmark reference. The model is simulated in Matlab/Simulink with the SimPowerSystem toolbox, and operated with the control strategy presented in section IV. Simulation results obtained with this model will be denoted as "AAM," since it can e considered as an Averaged Arm Model.

2) A non-linear state-space model including the derived SSTI representation of the MMC internal dqz dynamics, as depicted in Fig. 5. The parts of this model that represent the MMC dynamics are summarized in (35), while the assumed control system implementation and the included ac- and dc-side dynamics are briefly described in section IV and section V.A, respectively. Results from this model will be denoted as "DQZ".

3) The simplified time-invariant MMC model described in section III.C. This model is based on the zero-sequence components of the energy sum and the circulating

$$x = \begin{bmatrix} v_{o,d} & v_{o,q} & i_{v,d} & i_{v,q} & \gamma_d & \gamma_q & i_{o,d} & i_{o,q} & \varphi_d & \varphi_q & v_{PLL,d} & v_{PLL,q} & \varepsilon_{PLL} & \delta\theta_{PLL} & v_{dc} & v_{dc,f} & \rho_p & \cdots \end{bmatrix}$$

$$\cdots \quad p_{ac,m} \quad i_{c,z} \quad i_{c,d} \quad i_{c,q} \quad w_{\Sigma,z} \quad w_{\Sigma,d} \quad w_{\Sigma,q} \quad w_{\Delta,d} \quad w_{\Delta,q} \quad w_{\Delta z,d} \quad w_{\Delta z,q} \quad \kappa_{\Sigma,z} \quad \kappa_{\Sigma,d} \quad \kappa_{\Sigma,q} \quad \xi_d \quad \xi_q \quad \xi_z \end{bmatrix}^T \quad (39)$$

$$u = \begin{bmatrix} i^*_{vq} & |v_g| & \omega_g & i_{dc,s} & p^*_{ac} & v^*_{dc} & w^*_{\Sigma,d} & w^*_{\Sigma,q} & w^*_{\Delta,d} & w^*_{\Delta,d} & w^*_{\Delta z,d} & w^*_{\Delta z,d} & w^*_{\Sigma,z} \end{bmatrix} \quad (40)$$
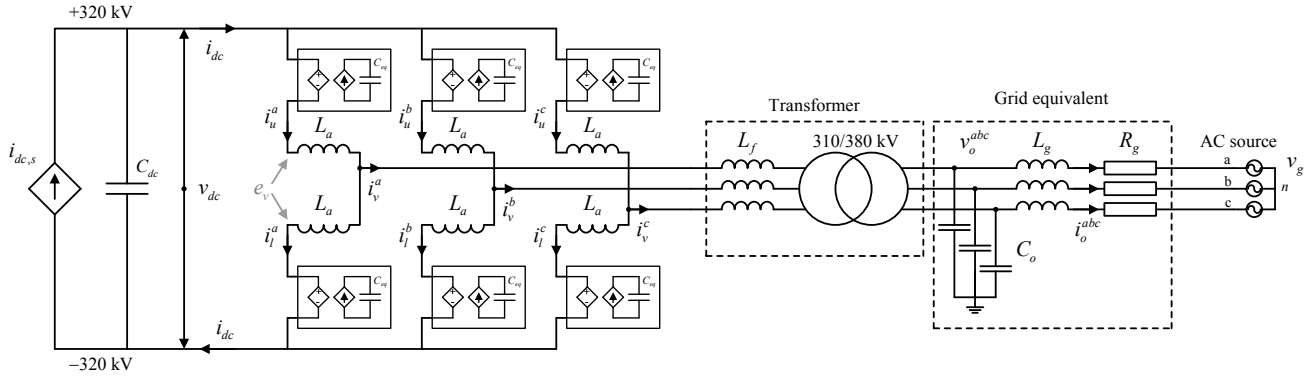
Fig. 7 Simulated reference model

current, as defined by (37), and corresponds to the model proposed in [25]. The ac- and dc-side dynamics included are the same as for the other models, and the simulated control system is a simplified version of what was discussed in section IV, resulting in the same control structure as discussed in [25]. An overview of the model is shown in Fig. 6, and results from the model will be denoted as "ZERO".

4) The small-signal state-space model obtained from linearization of the model in case 2. The model will be linearized at the initial steady-sate operating point of the detailed nonlinear model, and the values of the state variables will be calculated as $\mathbf{x} = \mathbf{x}_0 + \Delta \mathbf{x}$. Results obtained from this model will be denoted as "ssDQZ".

5) The small-signal model obtained from linearization of the model in case 3. The results will be presented in the same way as for case 4, and the results will be denoted as "ssZERO".

All simulations are based on the MMC HVDC terminal configuration shown in the previous figures, with parameters given in Table I. It should be noted that the ac-side inductance L_f for the MMC in this case is the equivalent leakage inductance of a transformer connecting the MMC to a simplified model of a 380 kV transmission system, as indicated in Fig. 7. Similarly, R_f is the equivalent series resistance of the transformer. In Table I, all parameters of the ac-system are referred to the converter-side of the transformer, since the transformer is explicitly represented only in the benchmark model. Furthermore, the equivalent arm capacitance C_{eq}

corresponds to an MMC with 400 sub-modules per arm, where each sub-module has a capacitance of about 8500 μF. Additionally, a droop gain of −10 pu determines the coupling between the dc voltage and the ac-side power reference.

It should be considered that the reference model is a conventional time-domain simulation model of a three-phase MMC representing arm or phase quantities, while the other 4 models with SSTI characteristics represent the MMC dynamics by variables transformed into a set of SRFs. Since the comparison of transient and steady-state responses is simpler with a SSTI representation, the results obtained from the reference model are transformed into the appropriate SRFs by using the phase angle from the simulated PLL. All results are plotted in per unit quantities, with base values derived from the nominal kVA rating of the MMC and the peak value of the nominal phase voltage, as specified in Table I.

To excite the MMC dynamics in the different models, a 10 % step reduction is introduced in the dc side current source $i_{dc,s}$, which is initially at 0.85 pu, corresponding to a dc power of 1.08 [pu]. The step is imposed at the simulation time $t = 0\ s$ and the current source is returned to its initial value at $t = 2\ s$.

The first set of results is presented in Fig. 8, for a case when the 2nd harmonic components of the energy sum are regulated to zero. In this figure, some of the variables which are common to all the simulated models are shown; i.e., the signals that are represented in both the "DQZ" and the "ZERO" models. These variables are, in Fig. 8 a); the zero-sequence energy sum $w_{\Sigma z}$, b) the zero-sequence of the circulating current i_{cz}, c) the voltage at the MMC dc terminals v_{dc}, d) the active component of the ac-

TABLE I PARAMETERS OF SIMULATED SYSTEM

| References [pu]		MMC Parameters				Per Unit System		Controller Parameters			
$w^{*}_{\Delta,}{}^{dqz+\omega}$	0	R_a	0.4915 Ω (0.5%)	L_g	0.0351 H (11.21%)	S_b	$V_n I_n \sqrt{3} = S_n$	$k_{p,iv}$	2.6010	$k_{p,w\Sigma dq}$	2
$w^{*}_{\Sigma d\text{-}2\omega}$	0	L_a	0.0250 H (8%)	R_g	0.0098 Ω (0.01%)	$V_b,\ I_b$	$\sqrt{2/3}\ V_{n,l\text{-}l},\ I_n \sqrt{2}$	$k_{i,iv}$	21.400	$k_{i,w\Sigma dq}$	2
$w^{*}_{\Sigma q\text{-}2\omega}$	0	L_f	0.0514 H (16.428%)	C_{eq}	25.904 uF (80%)	ω_b	$2\pi f_n$	$k_{p,cc}= k_{p,ccz}$	0.1114	$k_{p,w\Delta dq}$	2
$w^{*}_{\Sigma z}$	1.25²	R_f	0.2802 Ω (0.285%)	C_{dc}	1.672 uF (5.1637%)	$Z_b,\ L_b,\ C_b$	$V_b/I_b,\ Z_b/\omega_b,\ 1/(\omega_b Z_b)$	$k_{i,cc} = k_{i,ccz}$	2.1875	$k_{p,w\Delta zdq}$	0.2
$i_{dc,s}$	0.85	C_o	2.8721uF (8.87%)	f_n	50 Hz	$V_{bdc},\ I_{bdc}$	$2V_b,\ S_b/V_{bdc}$	$k_{p,w\Sigma z}$	10	$k_{p,pac}$	1
v^{*}_{dc}	1.25	$V_{n,l\text{-}l}$	313.5 kV$_{RMS}$	S_n	1000 MVA	$Z_{bdc},\ L_{bdc},\ C_{bdc}$	$V_{bdc}/I_{bdc},\ Z_b/\omega_b,\ 1/(\omega_b Z_b)$	$k_{i,w\Sigma z}$	10	$k_{i,pac}$	50
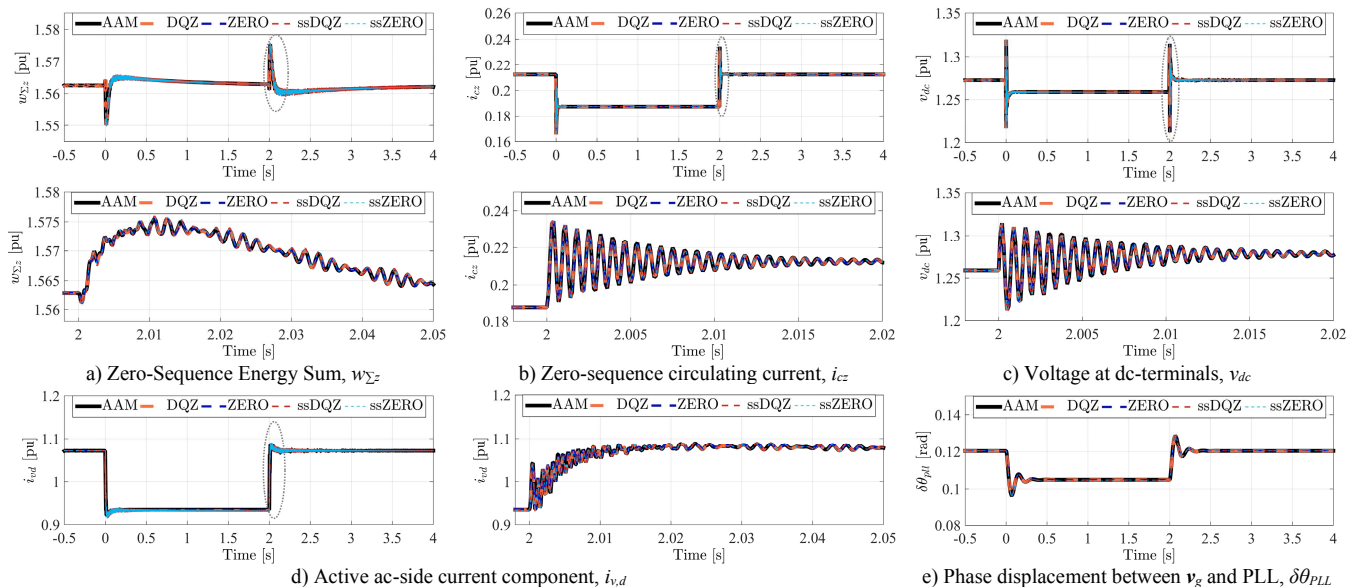
Fig. 8 Time-domain validation of time-invariant MMC models: Complete *dqz* and simplified zero-sequence model validation by comparison to MMC benchmark model with sum energy oscillations controlled to zero.

current (converter side) $i_{v,d}$, and e) the phase shift between the PLL orientation and the equivalent grid voltage, $\delta\theta_{PLL}$. From Fig. 8 it can be initially concluded that the detailed SSTI representation as well as the simplified zero sequence model (i.e. "DQZ" and "ZERO") obtain a high degree of accuracy, as they capture the dynamic response of the reference model without any noticeable deviation. The results presented in the figure also confirm that the model is accurate for both fast and slow dynamics. Similarly, their linearized small-signal versions ("ssDQZ" and "ssZERO") accurately capture the system dynamics, particularly for the event occurring at $t = 2$ s, as the system is then returning to the operating point around which it was linearized.

From the curves in Fig. 8, it can be noticed that energy sum reaches the desired value of 1.5625 in steady-state, which corresponds to the square of the desired dc terminal voltage; i.e., 1.25^2. This results from having a zero-sequence energy sum reference in real values defined as $W_{\Sigma z}{}^*=2(\frac{1}{2} C/N(1.25V_{dc,b})^2)$, and a base value for the energy defined as $W_{\Sigma b}=2(\frac{1}{2}C/N(V_{dc,b})^2)$. Thus, the energy base value corresponds to the energy in one phase when the upper and lower arm voltages are equal to the base value for the dc voltage. In addition to the zero-sequence energy, this energy base value is further used to scale the *dq* components of the energy sum, as well as all components of the energy difference. Moreover, it can be noticed that the circulating current settles to 0.2125 *pu* after $t = 2$ s, which corresponds to one fourth of the final value of i_{dcs}. This scaling is a result of applying the ac-side base value to the zero sequence circulating current, and the scaling of the Park transformation [14], [25].

Note that the simplified zero-sequence SSTI model does not require any information on how the 2nd harmonic circulating currents are controlled to provide an accurate representation of the macroscopic variables presented in Fig. 8, as long as the internal variables are stable and the losses associated with the internal MMC dynamics are negligible. Thus, the accuracy of the simplified model is not significantly influenced by whether a constant circulating current control strategy or a constant energy sum control is used.

By contrast, Fig. 9 shows the MMC energy state variables that have been neglected in the simplified zero-sequence model: the *dq*-components of a) the energy sum w_Σ, b) energy difference w_Δ, and c) zero-sequence energy difference $w_{\Delta z}$. In addition, the *dq*-components of the circulating current i_c are given in Fig. 10. The results in Fig. 9 and Fig. 10 demonstrate that the detailed SSTI model accurately captures the internal dynamics of the average model it was derived from. In addition, its linearized small-signal model is able to represent the dynamic behavior with high accuracy.

As a point of reference, the behavior of the circulating current, the energy sum and the energy difference in each phase have been plotted in Fig. 11-a), -b) and -c). These are exactly the same simulation results that have been transformed into their associated SRFs for the comparison of the models in Fig. 9 and Fig. 10. Since it was demonstrated that all the models provide the same results, only the reference model is plotted for the sake of clarity. The waveforms are as expected, with the energy settling to a constant value in steady state. Furthermore, it is worth noticing that all oscillating variables settle to balanced three-phase signals with a common average value in steady state, since their respective *dq*-components are controlled to constant values by the MMC controllers. Finally, Fig. 11 d) and e) show respectively the arm currents and aggregated voltages of the phase *a*, to illustrate the actual waveforms of the reference model. Indeed, the dc-component, the fundamental frequency component and the second harmonic component in the arm currents can be clearly seen from Fig. 11 d).

When studying the results in Fig. 11 e) in comparison to the results in From Fig. 9 and Fig. 10, it should be remembered that the actual waveform of the sum arm voltage is related to the sum arm energy, and the per phase sum energy and energy difference variables according to (5). Since the average value of the sum arm voltage is much higher than the oscillating components, the influence of the square root relationship

a) *d*- and *q*-axis components of the energy sum w_Σ

b) *d*- and *q*-axis components of the energy difference, w_Δ

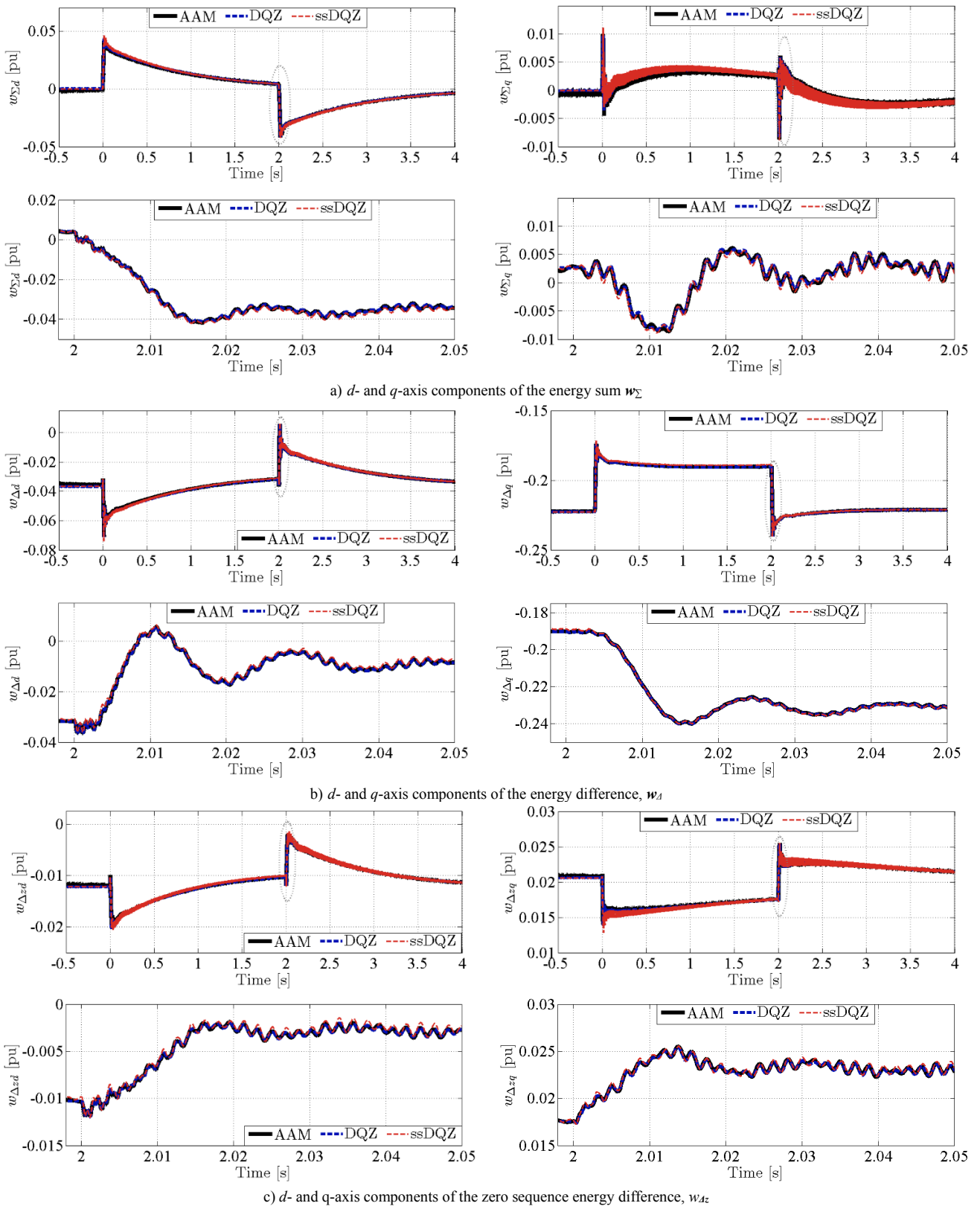c) *d*- and q-axis components of the zero sequence energy difference, $w_{\Delta z}$

Fig. 9 Time-domain validation of detailed SSTI representation of the internal MMC energy variables

between the sum arm energy and the sum arm voltage cannot be easily noticed from Fig. 11 e). Thus, it can be seen from the curves in Fig. 11 e) that the transient response in the equivalent sum arm voltage contains:

1) A dc-bias with its corresponding transients
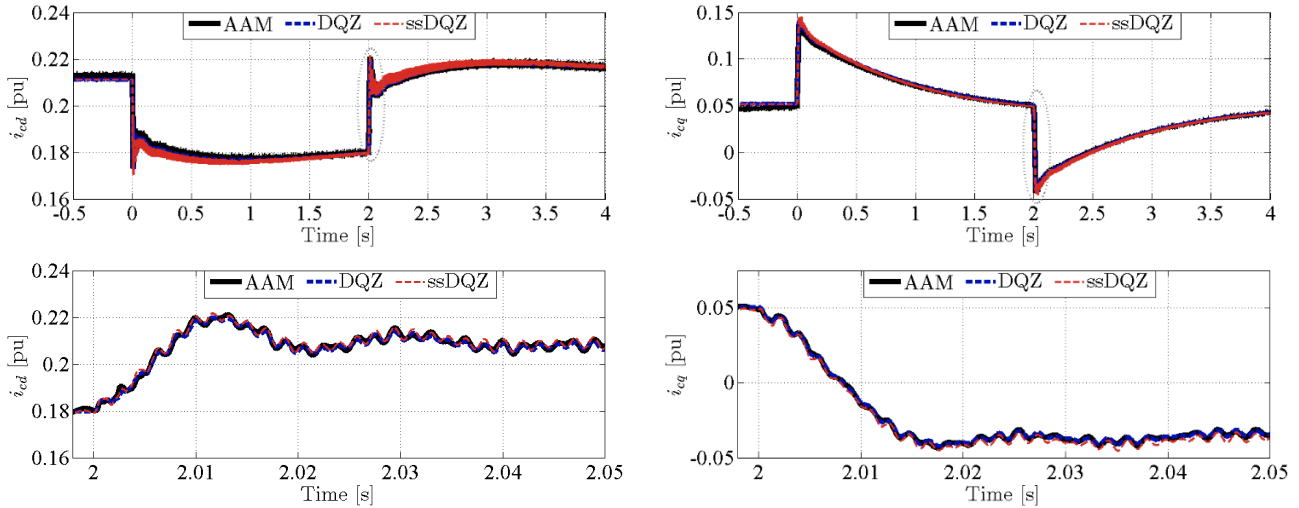2) A fundamental frequency component

Fig. 10 Time-domain validation of detailed SSTI representation of the d- and q-axis components of the internal circulating currents $\boldsymbol{i}_c$

a) Circulating Current in the three phases   b) Energy Sum for the three phases   c) Energy Difference for the three phases

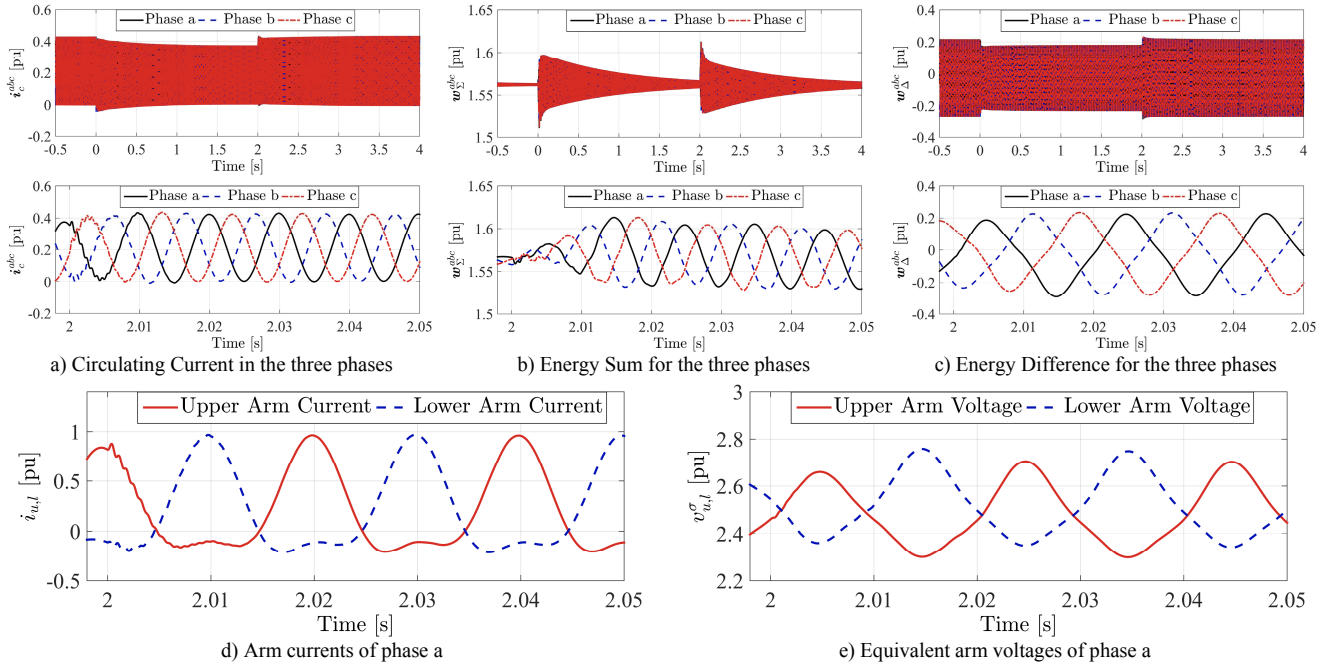d) Arm currents of phase a

e) Equivalent arm voltages of phase a

Fig. 11 MMC internal variables in the stationary $\Sigma\Delta$ representation, and an example of arm quantities obtained from the reference model

3) A second harmonic component (which in this case is slowly regulated to zero to reduce the capacitor voltage oscillations as seen from Fig. 11 b))

4) A third harmonic component.

From the results in Fig. 9 and Fig. 10, it should be clear that these components are all accurately represented in their appropriate SRFs by the derived SSTI state-space equations.
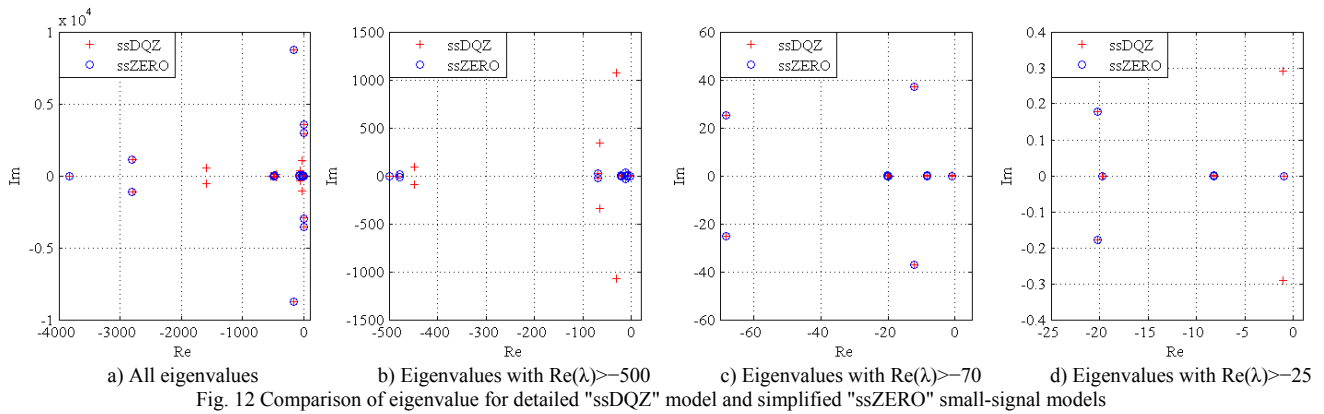
VII. ANALYSIS OF MMC SMALL-SIGNAL DYNAMICS

For demonstrating the potential applicability of the derived SSTI representation of the MMC, an example of small-signal eigenvalue analysis is presented in this section. This example will demonstrate how the nonlinear state-space model is necessary for calculating the steady-state operating point needed for linearization, and how the linearized small-signal model can be utilized for revealing the dynamic properties, sensitivities and stability limitations of the modelled system. It

is important to that note the obtained results rely on the SSTI modelling approach, and that similar results cannot be directly obtained from the conventional average model in the stationary reference frame.

A. Eigenvalue analysis for identifying sources of oscillations

As a first example of small-signal analysis, the eigenvalues are calculated for the small signal state-space model representing the detailed internal dynamics of the MMC as well as for the simplified model, when the system is linearized at the same operating point as used for the simulations in the previous section. The resulting eigenvalues are plotted in the complex plane for comparison, as shown in Fig. 12. From the various scales shown in Fig. 12 a)-d), it can be clearly seen that all eigenvalues that exist in the simplified "ssZERO" model are also present in the detailed "ssDQZ model." This clearly confirms that the simplifications associated with the zero

a) All eigenvalues   b) Eigenvalues with Re(λ)>−500   c) Eigenvalues with Re(λ)>−70   d) Eigenvalues with Re(λ)>−25

Fig. 12 Comparison of eigenvalue for detailed "ssDQZ" model and simplified "ssZERO" small-signal models

sequence model only implies that some of the system dynamics are not represented, while the dynamics included in the model accurately corresponds to the detailed model.

For further assessing the information that can be obtained from the small-signal models, the eigenvalues of the "ssDQZ" model are listed in Table II. This table also lists the time-constant T_i, the oscillation frequency f_i, and the damping factor ζ_i of each mode i, which are defined from the real and imaginary part of the eigenvalue, according to [14]:

$$\lambda_i = a_i \pm jb_i \;\rightarrow\; z_i(t) = z_{0,i}e^{a_it}\cos(b_i \cdot t + \theta_i),$$
$$T_i = \frac{1}{a_i}, \quad f_i = \frac{b_i}{2\pi}, \qquad \zeta_i = \frac{a_i}{\sqrt{a_i^2 + ab_i^2}}, \tag{42}$$

This equation also defines the general form of the time-response $z(t)$ associated with an individual mode λ_i.

By considering the transient responses resulting from the time-domain simulations, it can be confirmed how the oscillatory components in the SSTI state variables are each directly associated to one of the identified modes. The high frequency oscillation at about 1400 Hz which can be seen in the Fig. 8 c) and d) is, for instance directly corresponding to the oscillation mode given by the eigenvalues $\lambda_{2,3}$. Similarly, the relatively damped oscillation with a frequency slightly above 50 Hz which can be noticed in the zoomed plots of Fig. 9

corresponds to the mode defined by the eigenvalues $\lambda_{19,20}$.

Although it is possible to identify some distinct eigenvalues in the time-domain response of the system, this does not explicitly reveal which variables are involved in each oscillation model. Thus, participation factor analysis can be utilized to identify which states are contributing to the different modes [14]. Such analysis can reveal which state variables are involved in causing poorly damped oscillations or instability problems and indicate potential interactions between the various state variables. The results from such participation factor analysis are summarized in the rightmost column of Table II, where all state variables with a participation higher than 10 % are listed for each mode. For instance, it can be noticed that the eigenvalues with the highest time constant (i.e. longest settling time of the transient) in this case are associated with the voltages and currents on the ac-side ($\lambda_{4,5}$) and the integrator states of the energy controllers ($\lambda_{25,26}$, λ_{27}).

B. Assessment of small-signal dynamics in the full expected operating range

Since the non-linear SSTI state-space equations can be solved for any feasible combination of input variables, it can be utilized as starting point for assessing the small-signal stability characteristics of the system over its entire range of expected operating conditions. As an illustration, a case where the power

TABLE II EIGENVALUES OF THE DETAILED MMC MODEL AND THEIR MAIN PARTICIPATING STATES

| Mode		Time constant	Oscillation frequency	Damping factor	Main participating states
λ_1	-500.00	$0.0020\ s$	-	-	$v_{PLL,d}$
$\lambda_{2,3}$	$-170.21 \pm j\ 8767.56$	$0.0059\ s$	$1395\ Hz$	0.194	$v_{dc},\ i_{c,z}$
$\lambda_{4,5}$	$-0.51 \pm j\ 3536.14$	$1.9608\ s$	$562.89\ Hz$	0.000144	$v_{o,d},\ v_{o,q},\ i_{o,d},\ i_{o,q}$
λ_6	-3826.35	$2.614\ x10^{-4}\ s$	-	-	$i_{v,q}$
$\lambda_{7,8}$	$-4.85 \pm j\ 2948.66$	$0.2062\ s$	$469.3\ Hz$	0.00160	$v_{o,d},\ v_{o,q},\ i_{o,d},\ i_{o,q}$
$\lambda_{9,10}$	$-2795.41 \pm j\ 1136.14$	$3.577\ x10^{-4}\ s$	$180.8\ Hz$	0.926	$i_{v,d},\ v_{dc,f},\ w_{\Sigma z}$
$\lambda_{11,12}$	$-1586.00 \pm j\ 514.61$	$6.305\ x10^{-4}\ s$	$81.90\ Hz$	0.951	$i_{c,d},\ i_{c,q},\ w_{\Sigma d},\ w_{\Sigma q},\ w_{\Delta z,d},\ w_{\Delta z,q}$
$\lambda_{13,14}$	$-30.71 \pm j\ 1071.11$	$0.0326\ s$	$170.5\ Hz$	0.0287	$w_{\Sigma d},\ w_{\Sigma q},\ w_{\Delta z,d},\ w_{\Delta z,q}$
λ_{15}	-541.96	$0.0018\ s$	-	-	$i_{v,d},\ i_{o,d},\ v_{dc,f},\ p_{ac,m},\ i_{c,d},\ i_{c,q},\ w_{\Sigma z}\ ,w_{\Sigma d},\ w_{\Delta z,q},$
λ_{16}	-481.96	$0.0021\ s$	-	-	$v_{PLL,q}$
$\lambda_{17,18}$	$-448.26 \pm j\ 89.27$	$0.0022\ s$	$14.21\ Hz$	0.981	$p_{ac,m},\ i_{c,d},\ i_{c,q},\ w_{\Sigma z}\ ,w_{\Sigma d},\ w_{\Sigma q},\ w_{\Delta,d},\ w_{\Delta,q},\ w_{\Delta z,d}$
$\lambda_{19,20}$	$-63.90 \pm j\ 341.24$	$0.0156\ s$	$54.31\ Hz$	0.199	$w_{\Sigma d},\ w_{\Sigma q},\ w_{\Delta,d},\ w_{\Delta,q}$
$\lambda_{21,22}$	$-68.18 \pm j\ 25.16$	$0.0147\ s$	$4.004\ Hz$	0.938	$\rho_p,\ p_{ac,m},\ w_{\Sigma z},\ \xi_z$
$\lambda_{23,24}$	$-12.07 \pm j\ 37.15$	$0.0829\ s$	$5.912\ Hz$	0.309	$\varepsilon_{PLL},\ \delta\theta_{PLL}$
$\lambda_{25,26}$	$-1.03 \pm j\ 0.29$	$0.9709\ s$	$0.0462\ Hz$	0.963	$\kappa_{\Sigma d},\ \kappa_{\Sigma q},$
λ_{27}	-1.00	$1\ s$	-	-	$\kappa_{\Sigma z},$
$\lambda_{28,29}$	$-20.15 \pm j\ 0.18$	$0.0496\ s$	$0.0286\ Hz$	0.999	$\varphi_d,\ \varphi_q,\ \xi_z,$
λ_{30}	-19.74	$0.0507\ s$	-	-	$\varphi_d,\ \varphi_q,\ \xi_z,$
λ_{31}	-19.63	$0.0509\ s$	-	-	$\xi_d,\ \xi_q,$
$\lambda_{32,33}$	$-8.23 \pm j\ 0.00$	$0.1215\ s$	-	1	$\gamma_d,\ \gamma_q,$
λ_{34}	-19.63	$0.0509\ s$	-	-	$\xi_d,\ \xi_q$
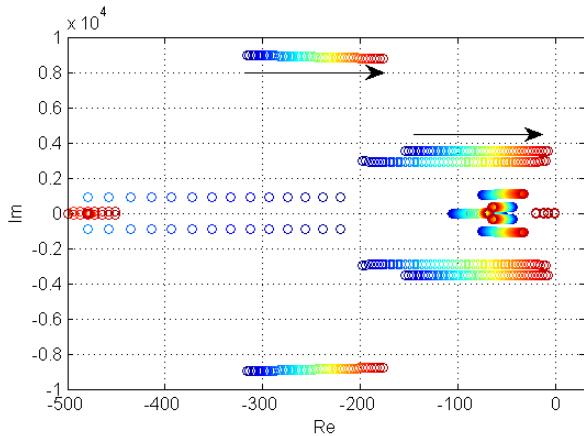
Fig. 13 Eigenvalue trajectory for operating conditions between $p_{ac}{}^* = -1.0$ pu (blue color) and $p_{ac}{}^* = 1.0$ pu (red color)

reference is changed from −1.0 pu to 1.0 pu, while the dc-side input current $i_{dc,s}$ is changed to provide a power equal to the reference value (i.e. $i_{dc,s} = p_{ac}{}^*/v_{dc}{}^*$) is studied and the results are presented in Fig. 13. This figure shows the trajectory of the eigenvalues with real part higher than −500 as the power flow is changed from −1.0 pu (blue color) to 1.0 pu (red color). The change of the eigenvalue locations can be considered as a measure of how the non-linearities of the system influence the small signal dynamics. Indeed, the results demonstrate that the system is approaching the stability limit when the power transfer is increasing. If the stability margin becomes very small, it will also indicate that any change of controller tuning or system parameters can easily cause stability problems.

C. Influence of internal variables on stability of the MMC

As demonstrated in section VI and VII.A, the simplified MMC state-space model is accurately representing the terminal dynamics of the MMC as long as all the internal dynamics are stable. However, the internal dynamics of the MMC can possibly compromise the overall system stability if the control loops are not tuned properly. Although the control systems used in this paper is a simplified implementation, the consequences of improper controller tuning can easily be demonstrated. As an example, Fig. 14 a) shows the eigenvalue trajectory when changing the gain of the controllers for the d- and q- axis energy sum from half of its initial value to 4 times its initial value from Table I. It can be seen from the figure that the system has one unstable mode for low values of the gain $k_{p,w\sum dq}$ (Mode A), and that another mode becomes unstable at very high values of $k_{p,w\sum dq}$ (Mode B).

Participation factor analysis is utilized to reveal the results of the instability identified in Fig. 14 a), and the results are plotted as bar diagrams for the two identified unstable modes in Fig. 14 b). This figure indicates that the Mode A instability is associated with a lack of control of the internal dynamics of the MMC due to the low gains, since the participating states are $w_{\sum d}$, $w_{\sum q}$, $w_{\Delta zd}$ and $w_{\Delta zq}$. However for high values of $k_{p,w\sum dq}$ the unstable mode (Mode B) is associated to the output voltage, the output current and the zero sequence sum energy $w_{\sum z}$. This indicates that a wrong tuning of the internal controllers can also cause stability problems to appear on the terminals of the MMC. Thus, the simplified zero-sequence model of the MMC should only be used when it can be assumed that the internal
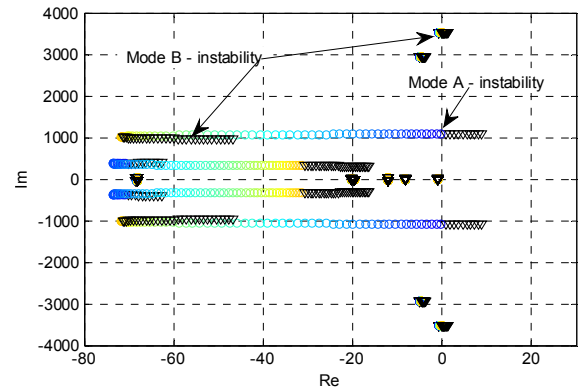

a) Eigenvalue trajectory for a change of $k_{p,w\sum dq}$ and $k_{i,w\sum dq}$ from 0.5 to 4 times the initial value (color gradient: blue to red) –black triangles denote instability
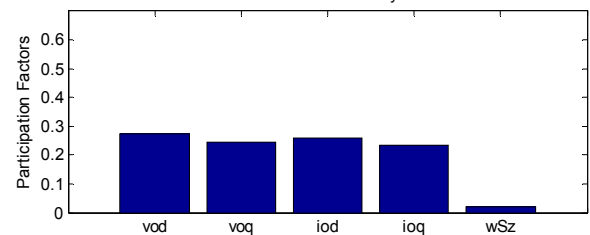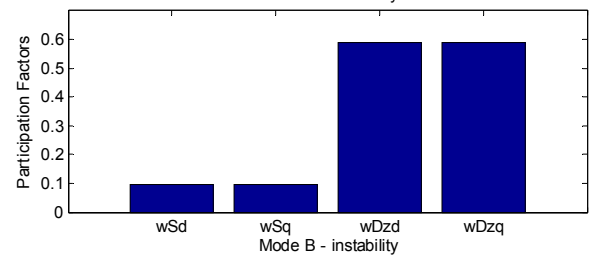
b) Participation factor analysis of the unstable eigenvalues at low values of $k_{p,w\sum dq}$ (Mode A) and at high values of $k_{p,w\sum dq}$ (Mode B)

Fig. 14 Example of eigenvalue analysis revealing potential instability of the MMC resulting from wrong tuning of the internal controllers
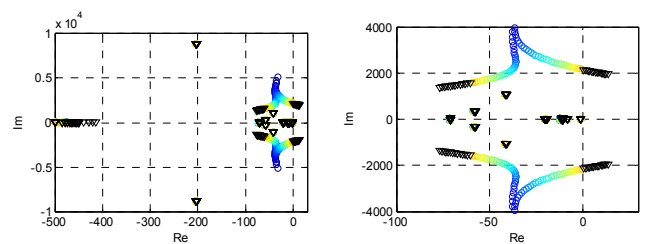
a) All eigenvalues with $Re(\lambda) > -500$ b) All eigenvalues with $Re(\lambda) > -100$

Fig. 15 Eigenvalue trajectory when changing the grid inductance l_g from 0.01 pu (blue color) to 0.6 pu. (orange/red color) – black triangles indicate instability

dynamics of the MMC are not causing any stability problems that can influence the overall operation of the system.

D. Sensitivity to operation under weak ac grid conditions

The developed SSTI models can also be utilized for evaluating the sensitivity with respect to parameter variations in the physical system or in the controller tuning. As an example of how external network parameters can influence the operation of the MMC, the impact of variations in the grid-side inductance of the assumed ac-system have been investigated. The eigenvalue trajectory resulting from changing the grid inductance between 0.01 pu and 0.6 pu are shown in Fig. 15. In this case, $i_{dc,s}$ is set to 0.5 pu and $p_{ac}{}^*$ is set to 0.4 pu, while all
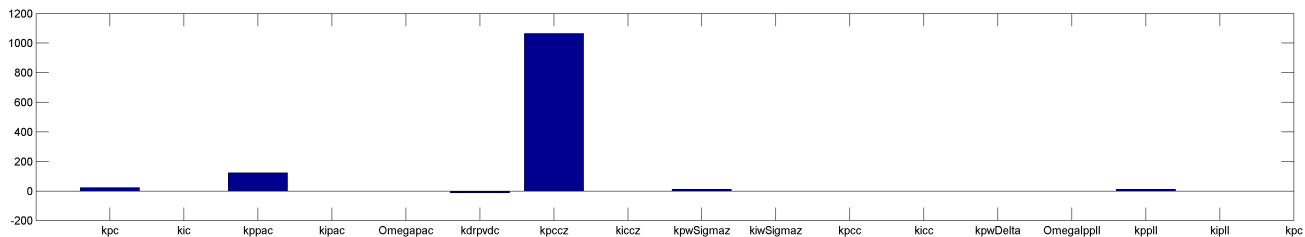
Fig. 16 Parametric sensitivity for critical eigenvalue causing instability with increasing grid inductance

other parameters are as given in Table I. From this figure, it can be seen that one of the eigenvalues previously identified to be associated with the ac-side electrical system is crossing into the right half-plane causing instability for high values of the grid inductance.

According to the results in Fig. 15, the control system should be re-tuned to ensure robustness with respect to the grid impedance for operating the MMC in weak grid conditions. For identifying the controller parameters that can be utilized to achieve a wider stability range, it is useful to calculate the parametric sensitivity of the eigenvalue causing the stability problems. The parametric sensitivity $\alpha_{n,k}$ of the eigenvalue λ_n to variations in parameter ρ_k is defined is defined as:

$$\alpha_{n,k} = \frac{\partial \lambda_n}{\partial \rho_k} = \frac{\boldsymbol{\Phi}_n^T \frac{\partial \mathbf{A}}{\partial \rho_k} \boldsymbol{\Psi}_n}{\boldsymbol{\Phi}_n^T \boldsymbol{\Psi}_n} \qquad (43)$$

where $\boldsymbol{\Psi}_n^T$ and $\boldsymbol{\Phi}_n$ are the left and right eigenvectors associated to the eigenvalue λ_n [14].

The real parts of the parametric sensitivity for the eigenvalues identified from Fig. 15 to cause instability have been calculated and are plotted in Fig. 16 for the case of a grid inductance of 0.6 pu (i.e. in the unstable region). From this figure, it can be seen that the eigenvalue location is especially sensitive to the value $k_{p,ccz}$ of the proportional gain for the zero sequence current controller, and to the value $k_{p,pac}$ for the proportional gain of the ac-side active power controller. Since the plots indicate the derivative of the eigenvalue real part with respect to the parameter, either of these parameters could be reduced to improve the stability of the system. This information allows for simple re-tuning of the controllers, since the location of the eigenvalues, and the parametric sensitivity can be easily recalculated after changing any parameter value.

By reducing the gains of $k_{p,cc,z}$ and $k_{p,pac}$ to 80 % of their initial values, it is possible to achieve a reasonable stability margin for the entire operating range for grid inductances up to 0.5 pu (i.e. SCR≈ 2). In case very high grid impedance values, the parameters of the PLL will also start to influence the stability of the system, as discussed in [37], but further investigations towards the ac-side grid interactions is beyond the scope of this paper.

An example of a time-domain simulation from the reference model described in section VI is presented in Fig. 17 to verify the results from the presented eigenvalue analysis. This figure shows a case with grid inductance of 0.5 pu, when the dc-side current $i_{dc,s}$ is increased from 0.4 pu to 0.5 pu, corresponding to a change of active power flow from about 0.5 pu to 0.62 pu. With the initial tuning of the system, labelled as Case A, the operation with $i_{dc,s}$ equal to 0.5 pu would be slightly beyond the stability limit according to Fig. 15, while
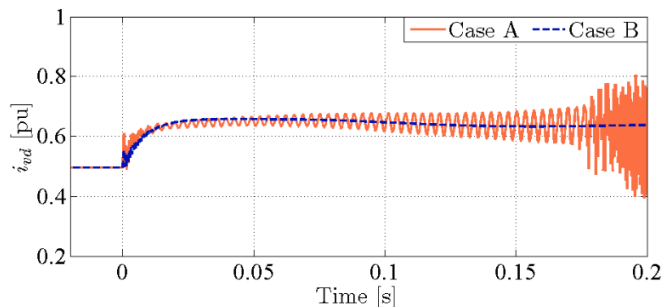

Fig. 17 Time domain verification of how system with initial tuning experiences stability problems as predicted by eigenvalue analysis during weak grid conditions and how re-tuned system maintains stability without significant oscillations

the operation with $i_{dc,s}$ of 0.4 could be found to be stable. This is clearly verified in the curve for Case A in Fig. 17, since the system is stable before the step in $i_{dc,s}$ while it becomes unstable with an increasing oscillation at about 310 Hz after the step. This oscillation frequency corresponds accurately to the imaginary part of the unstable eigenvalues from Fig. 15. The case with $k_{p,cc,z}$ and $k_{p,pac}$ reduced to 80 % of their initial values is labelled as Case B, and the result from simulating the same step in $i_{dc,s}$ for this case is also shown in Fig. 17, clearly verifying that the system has been stabilized.

VIII. CONCLUSIONS

This paper presents a modelling approach for obtaining a Steady-State Time-Invariant (SSTI) state-space representation of MMCs. The presented approach is suitable for MMCs with control strategies utilizing on-line compensation for the arm voltage oscillations in the calculation of the arm insertion indices, referred to in this paper as *compensated modulation*. The derived model captures the MMC internal dynamics while imposing steady-state time-invariance on each variable. This was achieved by an energy-based $\sum$-Δ formulation which enabled separation of the MMC variables according to their oscillation frequencies. A procedure for deriving equivalent SSTI *dqz* representation of all state variables by applying three different Park transformations was presented, referring each variable to its associated SRF, rotating at once, twice or three times the grid fundamental frequency. The resulting model can be suited for detail-oriented studies, as it captures the dynamics of the second harmonic circulating currents and the internal energy dynamics of the MMC.

The paper also demonstrates how the developed detailed model can be simplified due to the characteristics of the compensated modulation. This yields in a MMC representation based only on the zero-sequence of the energy-sum and the zero-sequence of the circulating current. This model corresponds to previously proposed MMC models for CM-

based control, derived by physical considerations and approximations, but the presented derivations provide explicit identification of the required simplifications. The simplified model is accurately representing the interface variables on the ac- and dc- side dynamics of the MMC, which are the main variables of concern from a macroscopic point of view and will be valid under the assumption that the neglected internal variables are properly tuned and therefore stabilized. Thus, this model is suited for power system-oriented studies.

The focus of this paper has been to derive SSTI models that can accurately represent the dynamics of a MMC, and a simplified control system was introduced only for verifying the derived models. Utilization of the presented models can enable a wide range of studies related to analysis and control system design for the MMC. As an example of applicability, the presented SSTI models have been linearized and assessed by means of small-signal eigenvalues-based techniques. For this purpose, the non-linear state-space models are needed to calculate the steady-state operating points for linearization according to the input variables and for obtaining the corresponding small-signal model. The resulting small-signal model calculated at any linearization point can be utilized for assessing the dynamic properties of the system. Thus, the small-signal model can be utilized for identifying potential stability problems or as a framework for improving the controller tuning and the performance of the system.

REFERENCES

[1] A. Lesnicar, R. Marquardt, "An innovative modular multilevel converter topology suitable for a wide power range, in *Proceedings of the 2003 IEEE Bologna PowerTech* Conference, Bologna, Italy, 23-26 June 2003, vol.3, pp. 272-277

[2] R. Adapa, "High-Wire Act: HVdc Technology: The State of the Art," in *IEEE Power and Energy Magazine*, vol.10, no.6, November/December 2012 pp.18-29

[3] J. Glasdam, J. Hjerrild, Ł. H. Kocewiac, C. L. Bak, " Review on Multi-Level Voltage Source Converter Based HVDC Technologies for Grid Connection of Large Offshore Wind Farms," in *Proceedings of the 2012 IEEE International Conference on Power System Technology*, POWERCON 2012, Auckland, New Zealand, 30 October – 2 November 2012, 6 pp.

[4] H. Akagi, "Classification, Terminology, and Application of the Modular Multilevel Cascade Converter (MMCC)" in *IEEE Trans.on Power Electronics*, vol. 26, no. 11, November 2013, pp. 3119-3130

[5] N. Ahmed, A. Haider, D. Van Hertem, L. Zhang, H.-P. Nee, "Prospects and Challenges of Future HVDC SuperGrids with Modular Multilevel Converters," in *Proceedings of the 2011 14th European Conference on Power Electronics and Applications*, EPE 2011, Birmingham, UK, 30 Aug. – 1 Sept. 2011, 10 pp.

[6] A. Antonopoulos, L. Ängquist, H.-P. Nee, "On Dynamics and Voltage Control of the Modular Multilevel Converter," in *Proceedings of the 13th European Conference on Power Electronics and Applications*, EPE'09, Barcelona, Spain, 8-10 September 2009, 10 pp.

[7] L. Harnefors, A. Antonopoulos, S. Norrga, L. Ängquist, H.-P Nee, "Dynamic Analysis of Modular Multilevel Converters," in *IEEE Trans. on Industrial Electronics*, vol. 60, no. 7, July 2013, pp. 2526-2537

[8] U. N. Gnanarathna, A. M. Gole, R. P. Jayasinghe, "Efficient Modeling of Modular Multilevel HVDC Converters (MMC) on Electromagnetic Transient Simulation Programs," in *IEEE Transactions on Power Delivery*, Vol. 26, No. 1, January 2011, pp. 316-324

[9] J. Peralta, H. Saad, S. Dennetière, J. Mahseredjian, S. Nguefeu, "Detailed and Averaged Models for a 401-Level MMC–HVDC System," in *IEEE Transactions on Power Delivery*, Vol. 27, No. 3, July 2012, pp. 1501-1508

[10] H. Saad, J. Peralta, S. Dennetière, J. Mahseredjian, J. Jatskevich, J. A. Martinez, A. Davoudi, M. Saeedifard, V. Sood, X. Wang, J. Cano, and Ali Mehrizi-Sani, "Dynamic Averaged and Simplified Models for MMC-Based HVDC Transmission Systems," in *IEEE Transactions on Power Delivery*, Vol. 28, No. 3, July 2013, pp. 1723-1730

[11] N. Ahmed, L. Ängquist, S. Norrga, A. Antonopoulos, L. Harnefors, H.-P. Nee, "A Computationally Efficient Continuous Model for the Modular Multilevel Converter" in *IEEE Journal of Emerging and Selected Topics in Power Electronics*, Vol. 2, No. 4, December 2014, pp. 1139-1148

[12] S. Rohner, J. Weber, S. Bernet, "Continuous Model of Modular Multilevel Converter with Experimental Verification," in *Proceedings of the 2011 IEEE Energy Conversion Congress and Exposition*, ECCE 2011, Phoenix, Arizona, USA, 17-22 September 2011, pp. 4021-4028

[13] N. R. Chaudhuri, R. Oliveira, Y. Yazdani, "Stability Analysis of Vector-Controlled Modular Multilevel Converters in Linear Time-Periodic Framework," in *IEEE Transactions on Power Electronics*, Vol. 31, No. 7, July 2016, pp. 5255-5269

[14] P. Kundur, "*Power System Stability and Control*," McGraw-Hill, New York, USA, 1994

[15] H. K. Khalil, "*Nonlinear Systems*," 3rd Edition, Prentice Hall, Upper Saddle River, New Jersey, USA, 2002

[16] S. R. Deore, P. B. Darji, A. M. Kulkarni, "Dynamic Phasor Modeling of Modular Multi-level Converters," in *Proceedings of the IEEE 7th International Conference on Industrial and Information Systems*, ICIIS 2012, Chennai, India, 6-9 August 2012, 6 pp.

[17] D. Jovcic, A. A. Jamshidifar, "Phasor Model of Modular Multilevel Converter With Circulating Current Suppression Control," in *IEEE Trans. on Power Delivery*, vol. 30, no. 4, August 2015, pp. 1889-1897

[18] S. Liu, Z. Xu, W. Hua, G. Tang, Y. Xue, "Electromechanical Transient Modeling of Modular Multilevel Converter Based Multi-Terminal HVDC Systems," in *IEEE Transactions on Power Systems*, vol. 29, no. 1, January 2014, pp. 72-83

[19] D. C. Ludois, G. Venkataramanan, "Simplified Terminal Behavioral Model for a Modular Multilevel Converter," in *IEEE Transactions on Power Electronics*, vol. 29, no. 4, April 2014, pp. 1622-1631

[20] N.-T. Trinh, M. Zeller, K. Wuerflinger, I. Erlich, "Generic Model of MMC-VSC-HVDC for Interaction Study with AC Power System," in *IEEE Transactions on Power Systems*, Vol. 31, No. 1, January 2016, pp. 27-34

[21] A. A. J. Far, "Circulating current suppression control dynamics and impact on MMC converter dynamics," in *Proc. of 2015 IEEE PowerTech*, Eindhoven, The Netherlands, 29 June – 1 July 2015, 6 pp.

[22] A. Jamshidifar, D. Jovcic, "Small Signal Dynamic DQ Model of Modular Multilevel Converter for System Studies," in *IEEE Transactions on Power Delivery*, Vol. 31, No. 1, February 2016, pp. 191-199

[23] V. Najmi, M. N. Nazir, R. Burgos, "A New Modeling Approach for Modular Multilevel Converter (MMC) in D-Q Frame," in *Proceedings of the 2015 IEEE Applied Power Electronics Conference and Exposition*, APEC 2015, Charlotte, North Carolina, USA, 15-19 March 2015, pp. 2710-2717

[24] T. Li, A. M. Gole, C. Zhao, "Harmonic Instability in MMC-HVDC Converters Resulting from Internal Dynamics," in *IEEE Transactions on Power Delivery*, Vol. 31, No. 4, August 2016, pp. 1738-1747

[25] G. Bergna Diaz, J. A. Suul, S. D'Arco, "Small-Signal State-Space Modeling of Modular Multilevel Converters for System Stability Analysis" in *Proceedings of the IEEE Energy Conversion Congress and Exposition*, ECCE 2015, Montreal, Quebec, Canada, 20-24 Sept. 2015, 8 pp.

[26] J. Freytes, L. Papangelis, H. Saad, P. Rault, T. Van Cutsen, X. Guillaud, "On the Modeling of MMC for use in Large Scale Dynamic Simulations," in *Proceedings of the 2016 IEEE Power System Computation Conference*, PSCC, Genoa, Italy, 20-24 June 2016, 7 pp.

[27] Q. Tu, Z. Xu, L. Xu, "Reduced Switching-Frequency Modulation and Circulating Current Suppression for Modular Multilevel Converters," in *IEEE Transactions on Power Delivery*, Vol.26, No.3, July 2011, pp.2009-2017

[28] L. Ängquist, A. Antonopoulos, D. Siemaszko, K. Ilves, M. Vasiladiotis, H.-P. Nee, "Open-Loop Control of Modular Multilevel Converters Using Estimation of Stored Energy," in *IEEE Transactions on Industry Applications*, Vol, 47, No. 6, November/December 2011, pp. 2516-2524

[29] G. Bergna Diaz, J. A. Suul, S. D'Arco, "State-Space Modelling of Modular Multilevel Converters for Constant Variables in Steady-State" in *Proceedings of the 2016 IEEE 17th Workshop on Control and Modeling for Power Electronics (COMPEL)*, Trondheim, Norway, 27-29 June 2016, 9 pp.

[30] G. Bergna, A. Garces, E. Berne, P. Egrot, A. Arzande, J.-C. Vannier, M. Molinas, "A Generalized Power Control Approach in ABC Frame for Modular Multilevel Converter HVDC Links Based on Mathematical Optimization," in *IEEE Transactions on Power Delivery*, vol.29, no.1, Feb. 2014, pp. 386-394

[31] R. Teodorescu, M. Liserre, P. Rodríguez, "*Grid Converters for Photovoltaic and Wind Power Systems,*" IEEE/John Wiley & Sons, Chichester, UK, 2011

[32] S. D'Arco, J. A. Suul, M. Molinas, "Implementation and analysis of a control scheme for damping of oscillations in VSC-based HVDC grids," in *Proceedings of the* 16th *International Power Electronics and Motion Control Conference and Exposition*, PEMC 2014, Antalya, Turkey, 21-24 September 2014, pp. 586-593

[33] H. Saad, X. Guillaud, J. Mahseredjian, S. Dennetière, S. Nguefeu, "MMC Capacitor Voltage Decoupling and Balancing Controls," in *IEEE Trans. on Pow. Delivery*, Vol. 30, No. 2, April 2015, pp. 704-712

[34] J. Freytes, G. Bergna, J. A. Suul, S. D'Arco, H. Saad, X. Guillaud, "State-space modelling with Steady-State Time Invariant Representation of Energy Based Controllers for Modular Multilevel Converters," in *Proceedings of the 12th IEEE PES PowerTech Conference*, Manchester, UK, 18-22 June 2017, 7 pp.

[35] G. O. Kalcon, G. P. Adam, O. Anaya-Lara, S. Lo, K. Uhlen, "Small-signal stability analysis of multi-terminal VSC-based DC transmission systems," in *IEEE Transactions on Power Systems*, vol. 27, no. 4, November 2012, pp. 1818-1830

[36] J. Beerten, S. D'Arco, J. A. Suul, "Identification and Small-Signal Analysis of Interaction Modes in VSC MTDC Systems," in *IEEE Trans. on Power Delivery*, Vol. 31, No. 2, April 2016, pp. 888-897

[37] J. Z. Zhou, H. Ding, S. Fan, Y. Zhang, A. M. Gole, "Impact of Short-Circuit Ratio and Phase-Locked-Loop Parameters on the Small-Signal Behavior of a VSC-HVDC Converter," in *IEEE Transactions on Power Delivery*, Vol. 29, No. 5, October 2014, pp. 2287-2296

Gilbert Bergna-Diaz received his electrical power engineering degree from the Simón Bolívar University, in Caracas, Venezuela, in 2008, a "Research Master" from "SUPÉLEC" (*École Supérieure d'Électricité*), in Paris, France, in 2010; and a joint PhD degree between SUPÉLEC and the Norwegian University of Science and Technology (NTNU) in 2015.

In March 2014 he joined SINTEF Energy Research as a research scientist, working on topics related to modeling and control of HVDC transmission systems. From August 2016 he started a post-doctoral fellowship at NTNU, working on control and modelling of power electronic systems.

Jon Are Suul (M'11) received the M.Sc. degree in energy and environmental engineering and the Ph.D. degree in electric power engineering from the Norwegian University of Science and Technology (NTNU), Trondheim, Norway, in 2006 and 2012, respectively.

From 2006 to 2007, he was with SINTEF Energy Research, Trondheim, where he was working with simulation of power electronic converters and marine propulsion systems until starting his PhD studies. From 2012, he resumed a position as a Research Scientist at SINTEF Energy Research, first in part-time position while also working as a part-time postdoctoral researcher at the Department of Electric Power Engineering of NTNU until 2016. His research interests are mainly related to analysis and control of power electronic converters in power systems and for renewable energy applications.

Salvatore D'Arco received the M.Sc. and Ph.D. degrees in electrical engineering from the University of Naples "Federico II," Naples, Italy, in 2002 and 2005, respectively.

From 2006 to 2007, he was a postdoctoral researcher at the University of South Carolina, Columbia, SC, USA. In 2008, he joined ASML, Veldhoven, the Netherlands, as a Power Electronics Designer, where he worked until 2010. From 2010 to 2012, he was a postdoctoral researcher in the Department of Electric Power Engineering at the Norwegian University of Science and Technology (NTNU), Trondheim, Norway. In 2012, he joined SINTEF Energy Research where he currently works as a Research Scientist. He is the author of more than 50 scientific papers and is the holder of one patent. His main research activities are related to control and analysis of power-electronic conversion systems for power system applications, including real-time simulation and rapid prototyping of converter control systems.